

Article

Archean Crustal Evolution of the Alxa Block, Western North China Craton: Constraints from Zircon U-Pb Ages and the Hf Isotopic Composition

Pengfei Niu ¹, Junfeng Qu ^{2,*}, Jin Zhang ², Beihang Zhang ²  and Heng Zhao ²

¹ Chengdu Exploration and Development Research Institute of PetroChina Daqing Oilfield Co., Ltd., Chengdu 610000, China; niupf92@163.com

² Institute of Geology, Chinese Academy of Geological Sciences, Beijing 100044, China

* Correspondence: qujf@cags.ac.cn

Abstract: The Alxa Block is an important component of the North China Craton, but its metamorphic basement has been poorly studied, which hampers the understanding of the Alxa Block and the North China Craton. In this study, we conducted geochronological and geochemical studies on three TTG (tonalite–trondhjemite–granodiorite) gneisses and one granitic gneiss exposed in the Langshan area of the eastern Alxa Block to investigate their crustal evolution. The zircon U-Pb dating results revealed that the protoliths of the TTG and granitic gneisses were formed at 2836 ± 20 Ma, 2491 ± 18 Ma, 2540 ± 38 Ma, and 2763 ± 42 Ma, respectively, and were overprinted by middle–late Paleoproterozoic metamorphism (1962–1721 Ma). All gneiss samples had high Sr/Y ratios (41–274) and intermediate Mg[#] values (44.97–55.78), with negative Nb, Ta, and Ti anomalies and moderately to strongly fractionated REE patterns ($(\text{La}/\text{Yb})_{\text{N}} = 10.6\text{--}107.1$), slight Sr enrichment, and positive Eu anomalies, displaying features of typical high-SiO₂ adakites and Archean TTGs. The magmatic zircons from the 2.84 Ga and 2.49 Ga TTG rocks had low $\epsilon_{\text{Hf}}(\text{t})$ values of $-1.9\text{--}1.7$, and $-3.83\text{--}2.12$ with two-stage model ages (T_{DMC}) of 3.24–3.11 Ga and 3.10–3.01 Ga, respectively, whereas those from the 2.54 Ga TTG rock exhibited $\epsilon_{\text{Hf}}(\text{t})$ values ranging from -1.1 to 3.46 and T_{DMC} from 3.0 Ga to 2.83 Ga, suggesting that the crustal materials of the basement rocks in the eastern Alxa Block were initially extracted from the depleted mantle during the late Paleoarchean to Mesoarchean era and were reworked in the late Mesoarchean and late Neoarchean era. By contrast, the Alxa Block probably had a relative younger crustal evolutionary history (<3.24 Ga) than the main North China (<3.88 Ga), Tarim (<3.9 Ga), and Yangtze (<3.8 Ga) Cratons and likely had a unique crustal evolutionary history before the early Paleoproterozoic era.



Citation: Niu, P.; Qu, J.; Zhang, J.; Zhang, B.; Zhao, H. Archean Crustal Evolution of the Alxa Block, Western North China Craton: Constraints from Zircon U-Pb Ages and the Hf Isotopic Composition. *Minerals* **2023**, *13*, 685. <https://doi.org/10.3390/min13050685>

Academic Editors: Jin Liu, Jiahui Qian, Xiaoguang Liu and Alexandre V. Andronikov

Received: 24 March 2023

Revised: 4 May 2023

Accepted: 15 May 2023

Published: 17 May 2023



Copyright: © 2023 by the authors. Licensee MDPI, Basel, Switzerland. This article is an open access article distributed under the terms and conditions of the Creative Commons Attribution (CC BY) license (<https://creativecommons.org/licenses/by/4.0/>).

1. Introduction

Tonalite–trondhjemite–granodiorite (TTG) rocks constitute a major part of Archean continental crust and provide information about the composition, tectonic environment, and evolution of the early continental crust [1,2]. Studies have shown that the early Precambrian era was an important period of crustal growth, the continental crust formed between 3.0 Ga and 2.5 Ga accounted for 36% of the present continental crust, and the continental crust formed during 2.15–1.65 Ga accounted for 39% [3]. There are two views stating that Precambrian crustal growth was concentrated in three main stages: either 3.6 Ga, 2.7 Ga, and 1.8 Ga or 2.7 Ga, 1.9 Ga, and 1.2 Ga [3,4].

The China continent mainly consists of three early Precambrian nuclei, including the Yangtze Craton (YC), Tarim Craton (TC), and North China Craton (NCC) (Figure 1) [5–10]. In recent decades, major progress has been made in the reconstruction of the crustal growth history of the YC and TC [11–16]. Paleoarchean (3437–3262 Ma) TTG rocks have been found in the YC with two-stage Hf model ages from Hadean to Eoarchean [17–21].

Recently, Eoarchean (ca. 3.7 Ga) TTG rocks have been identified from the TC [22]. Additionally, the oldest detrital zircons from the basement rocks of the two cratons were dated 3.8–3.2 Ga with Eoarchean to Paleoarchean two-stage Hf model ages from the Eoarchean to Paleoarchean era [23–25], which suggest that the crustal evolution of the two cratons had already begun before the Paleoarchean era.

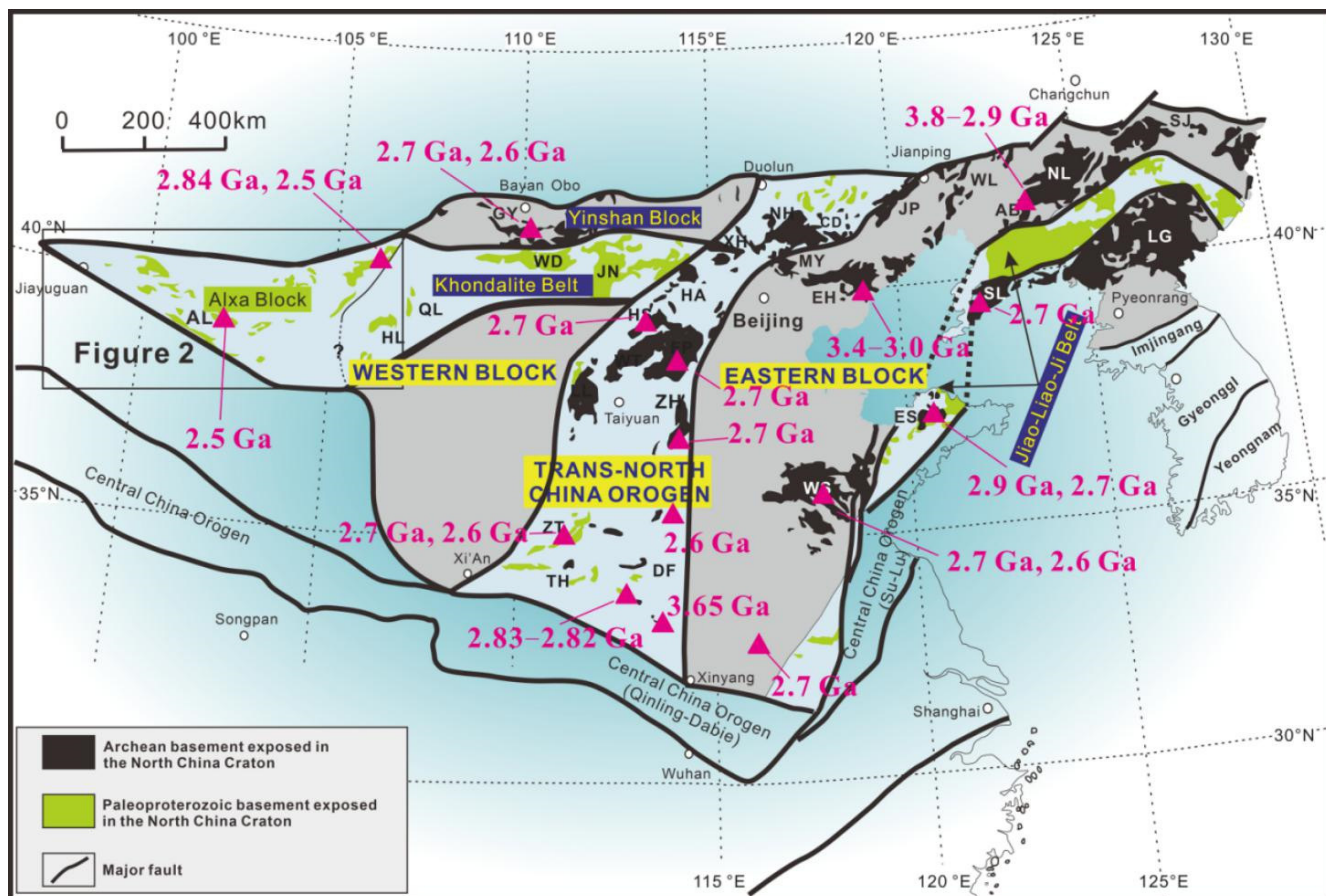


Figure 1. Distribution of Precambrian basement and subdivision of the North China Craton [26–28]. Additionally, shown are the locations of Archean TTGs with rock ages.

As one of the oldest cratons in China, the North China Craton (NCC) experienced a long and complicated geological history [29–32]. Most present models divide the NCC into the Eastern Block, Western Block, and Trans North China Orogen (TNCO) [27,33] (Figure 1). The early Precambrian tectonic pattern of the NCC remains controversial. Some scholars have believed that cratonization was completed ca. 2.5 Ga, marked by the “Wutai Movement” [34,35], followed by regional extension at the end of the Paleoproterozoic era that resulted in the destruction of the NCC (called activation) [36], while others have believed that the basement of the NCC had not been completely consolidated until ca. 1.9 Ga [37–40], and the “Lvliang Movement” ca. 1.8 Ga caused the Eastern Block and Western Block of the NCC to join together along the TNCO [7,41].

The Alxa Block is located in the westernmost part of the NCC. Compared with the main NCC and the YC and TC, the Precambrian basement of the Alxa Block is relatively less studied, which restricts a better understanding of the evolution of the NCC. In this paper, we report new geochronological and geochemical results for Meso-Neoarchean rocks from the Langshan area, which confirm the existence of the Archean basement in the Alxa Block and reveal evidence for the crustal evolution of the NCC.

2. Geological Background and Sample Descriptions

The Alxa Block, as the westernmost part of the NCC, is adjacent to the Central Asian Orogenic Belt in the north, the TC in the west, and the North Qilian Orogenic Belt in the south. The Precambrian basement of the Alxa Block is mainly exposed in the Longshoushan, Beidashan, Yabulaishan, Bayanwulashan, and Langshan areas (Figure 2), and the Bayanwula–Langshan Fault in the east is considered the eastern boundary of the Alxa Block [42,43]. The wide distribution of deserts and limited basement outcrops in the Alxa Block hamper the understanding of its tectonic pattern. The NE-oriented Langshan Mountains, located on the northeastern margin of the Alxa Block (Figure 2), are key areas in unravelling the early Precambrian geological evolution between the NCC and Alxa Block.

As the oldest basement in the Langshan area, the Diebusige Complex is mainly composed of banded biotite plagioclase gneiss, amphibolite gneiss, magnetite quartzite, marble, intrusive k-feldspar granite, and amphibolite. Some chronological studies have been conducted on the Diebusige Complex, but the formation age of the Diebusige Complex remains uncertain. Yang et al. (1988) [44] determined that the Rb-Sr isochron age of amphibolite was 3219 Ma, while Li et al. (2006) [45] obtained a Sm-Nd isochron age of 3081 ± 49 Ma, suggesting that the Diebusige Complex was formed in the Paleo-Mesoarchean era. The 2.75–3.5 Ga ages of detrital zircons and 2.5–2.69 Ga, 1.9–1.95 Ga, and 1.8–1.85 Ga ages of metamorphic zircons that Geng et al. (2006, 2007, 2010) [46–49] obtained from the Diebusige gneisses indicated that they were formed in the Neoarchean and underwent tectono-thermal events in the late Neoarchean and late Paleoproterozoic era. Dan et al. (2012) [50] suggested that the supracrustal rocks of the Diebusige Complex were deposited at 2.0–2.45 Ga and experienced metamorphism at 1.89 Ga and 1.79 Ga. Based on the chronology of the metamorphic basement, they believed that there was no Archean rock exposed in the eastern Alxa Block. However, Gong et al. (2012) [51] and Zhang et al. (2013) [52] found ca. 2.5 Ga TTG rock in the Beidashan area, providing evidence for the existence of exposed Archean rocks in the Alxa Block.

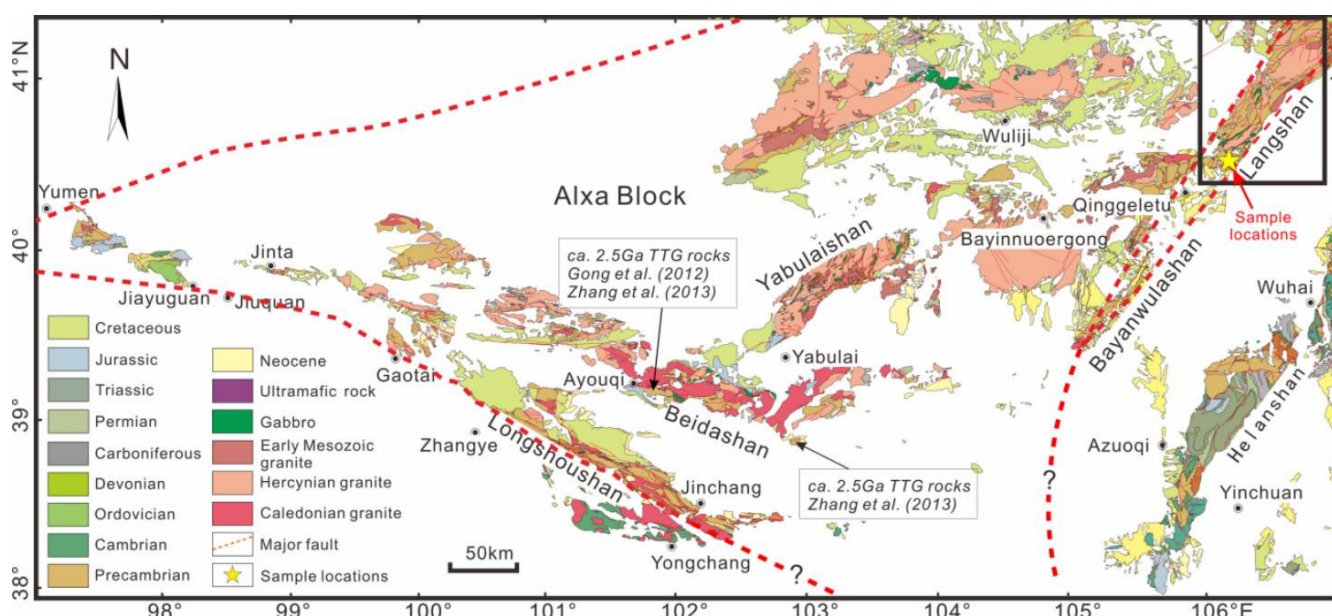


Figure 2. Geological map of the Alxa Block, westernmost North China Craton, and basement distribution of the Alxa Block. The ca. 2.5 Ga TTG rocks exposed in Beidashan area are from references [51,52].

Three TTG gneiss samples and one granitic gneiss sample were selected from the Diebusige Complex for this study; their detailed locations are shown in Table 1. All samples are gray-white, fine-to-medium grained, and generally show gneissic fabrics. Mineral grains are subhedral to anhedral, and some show serrated boundaries (Figure 3). The

tonalitic gneiss (1810-1) mainly consists of plagioclase, quartz, hornblende, and minor biotite. Hornblende grains show recrystallization fronts, and quartz grains show irregular and crenulated margins, which suggests dynamic recrystallization. The trondhjemite gneiss (1814-3) is mainly composed of plagioclase, quartz, hornblende, minor biotite, and K-feldspar. It was strongly affected by later deformation, and plagioclase and hornblende showed different degrees of fragmentation and alteration. Another tonalitic gneiss (1816-1) is characterized by a typical mineral assemblage of plagioclase, quartz, hornblende and biotite. Plagioclase grains show polysynthetic twinning, and quartz occurs as fine-grained and anhedral grains. Hornblende is the major dark mineral, and recrystallization is apparent in the surrounding area. The granitic gneiss (D798) is mainly composed of quartz, plagioclase, and biotite with minor accessory minerals of apatite, and mylonitization occurs under the superposition of later tectonic events.

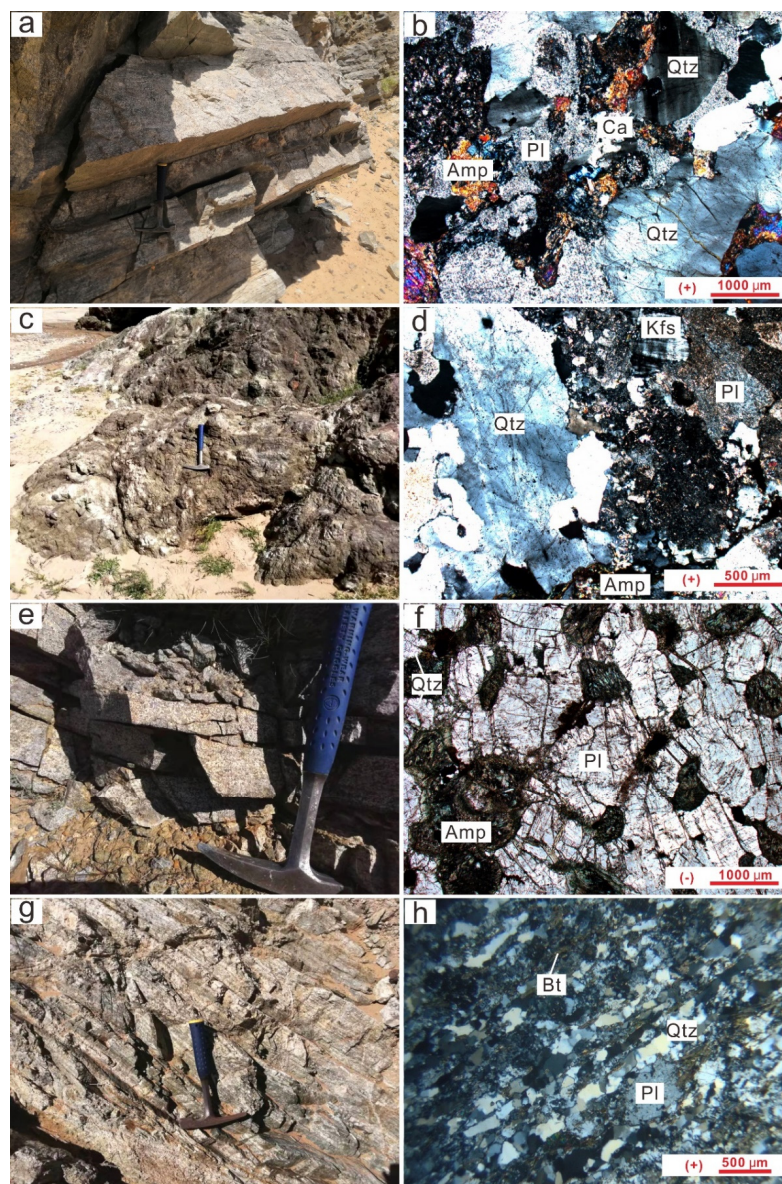


Figure 3. Field photos and representative photomicrographs of the TTG rocks and granitic samples from the Diebusige Complex, eastern Alxa Block. (a,b) Tonalitic gneiss sample 1810-1; (c,d) trondhjemite gneiss sample 1814-3; (e,f) tonalitic gneiss sample 1816-1; and (g,h) granitic gneiss sample D798. Qtz: quartz; Pl: plagioclase; Bt: biotite; Kfs: K-feldspar; Amp: amphibole; and Ca: calcite.

Table 1. GPS locations and lithology of the representative samples.

Sample	GPS Location	Lithology	Mineral Assemblage
1810-1	40°35'55.15'' N 106°16'42.56'' E	Tonalitic gneiss	Qtz (25%) + Pl (65%) + Hb (5%) + Bt (5%)
1814-3	40°35'53.69'' N 106°16'53.29'' E	Trondhjemite gneiss	Qtz (35%) + Pl (45%) + Hb (10%) + Bt (5%) + Kfs (5%)
1816-1	43°34'20.01'' N 106°12'29.44'' E	Tonalitic gneiss	Qtz (20%) + Pl (60%) + Hb (15%) + Bt (5%)
D798	40°35'19.14'' N 106°15'38.23'' E	Granitic gneiss	Qtz (30%) + Pl (55%) + Bt (15%)

3. Analytical Methods

3.1. Geochemistry

Whole-rock major and trace element analyses were completed at Wuhan Sample Solution Analytical Technology Co., Ltd. (Wuhan, China), and external standards and repeated samples were used to comprehensively control the analytical quality. Whole-rock major elements were measured using XRF, and five standards, BHVO-2, GSP-2, W-2A, GBW07103 and GBW07316, were determined in parallel. Trace elements were analyzed by inductively coupled plasma–mass spectrometry (ICP–MS) on an Agilent 7700e instrument with a shielded torch, and four standards, AGV-2, BHVO-2, BCR-2 and RGM-2, were used to monitor the analytical quality. The relative standard deviations for the whole-rock major and trace elements are within $\pm 5\%$.

3.2. Zircon U-Pb Dating and Hf Isotopic Composition

SHRIMP zircon U-Pb dating was performed using a sensitive high-resolution ion microprobe (SHRIMP-II) at the Beijing SHRIMP Center, Institute of Geology, Chinese Academy of Geological Sciences, Beijing. The analytical procedure was the same as that of Williams. (1998) [53]. The primary flow intensity was 4.5 nA, and the spot size was 25–30 μm . Standard zircon TEM (417 Ma) was used for the age corrections [54]. Data processing was carried out using the ISOPLOT program [55], and uncertainties for individual analyses were quoted at 1σ , whereas those for weighted mean ages were quoted at a 2σ and 95% confidence level.

Zircon in situ Lu-Hf analyses were carried out using an NU plasma II MC-ICP–MS at the School of Earth and Space Sciences, Peking University. An ArF-excimer laser ablation system of Geolas HD (193 nm) was used with a 44 μm spot size. The analytical procedure was the same as that of Zhang et al. (2016) [56]. Data reduction was conducted using the IOLITE program [57]. Zircon 91,500 was used as an internal standard with a reference value of $^{176}\text{Hf}/^{177}\text{Hf} = 0.282307 \pm 31$ (2SD) [58], zircon Plešovice was used as the monitoring standard, and the value of $^{176}\text{Hf}/^{177}\text{Hf} = 0.282483$ (2SD) was obtained, which was consistent with the suggested value of 0.282482 ± 13 (2SD) [59].

4. Results

4.1. Whole-Rock Major and Trace Elements

Whole-rock major and trace element analyses were performed on four samples, including three TTG gneisses (1810-1, 1814-3, and 1816-1) and one granitic gneiss (D798). The analytical results are given in Table 2.

4.1.1. Major Element Geochemistry

The TTG gneisses from the Diebusige Complex in the Langshan area had SiO_2 contents of 60.55–77.80 wt.%, Al_2O_3 contents of 10.90–19.11 wt.%, and $\text{Na}_2\text{O}/\text{K}_2\text{O}$ ratios of 0.93–6.38. In the normative An-Ab-Or diagram (Figure 4a), the samples 1810-1 (2.84 Ga) and 1816-1 (2.54 Ga) plotted in the tonalite field, except for sample 1814-3 (2.49 Ga), which plotted in the trondhjemite field. According to the A/NK vs. A/CNK classification (Figure 4b),

the two tonalitic gneisses were weakly metaluminous, while the trondhjemite gneiss was weakly peraluminous, which was in line with the TTG rocks with corresponding ages in the NCC. All TTG gneisses showed features of subalkaline series in the TAS diagram (Figure 4c). They mainly plotted in the medium-to-low K fields of the calc-alkaline and tholeiitic series in the K_2O vs. SiO_2 diagram (Figure 4d). In addition, they had $Mg^{\#}$ values ranging between 44.97 and 52.23, with an average of 49.96 (Table 2), slightly higher than those of Archean high-Al TTGs (42 on average).

Table 2. Analytical results of major (.wt%) and trace (ppm) elements for TTG and granitic gneisses in the eastern Alxa Block.

Sample	D798							1810-1		1814-3			1816-1		
Rock Type	Granitic Gneiss							Tonalitic Gneiss	Trondhjemite Gneiss			Tonalitic Gneiss			
SiO ₂	69.84	71.54	72.30	71.67	64.18	66.78	68.86	71.88	77.80	69.41	60.55	66.49	66.14	62.04	68.71
TiO ₂	0.23	0.18	0.21	0.36	0.30	0.41	0.30	0.20	0.05	0.42	0.08	0.18	0.64	0.81	0.41
Al ₂ O ₃	15.10	13.68	12.11	12.58	15.99	15.64	16.1	13.71	10.90	12.17	19.11	14.64	14.86	14.32	13.13
TFe ₂ O ₃	1.71	1.48	1.60	2.61	2.90	3.28	2.06	1.72	1.39	4.66	4.06	4.80	5.26	7.73	4.32
MnO	0.03	0.03	0.03	0.04	0.05	0.05	0.03	0.02	0.02	0.07	0.06	0.07	0.09	0.11	0.07
MgO	1.09	0.71	0.76	1.26	1.55	1.64	0.88	0.88	0.76	2.54	2.24	2.56	2.17	3.21	2.37
CaO	1.30	1.87	2.33	2.13	2.61	1.96	2.99	1.12	3.73	1.79	1.50	1.73	4.19	5.00	4.94
Na ₂ O	3.89	3.05	2.85	4.14	3.68	4.13	5.35	3.28	2.81	4.03	6.77	4.46	3.66	3.44	3.61
K ₂ O	4.07	4.62	4.81	2.75	5.08	3.48	1.80	5.14	1.33	2.02	2.94	1.90	1.20	0.84	0.57
P ₂ O ₅	0.02	0.01	0.07	0.08	0.28	0.10	0.13	0.01	0.06	0.07	0.13	0.08	0.14	0.11	0.14
LOI	2.56	2.66	2.74	2.22	3.03	2.32	1.17	1.77	1.47	2.60	2.30	2.90	1.46	2.19	1.61
total	99.84	99.83	99.80	99.84	99.64	99.77	99.74	99.72	100.32	99.77	99.73	99.81	99.81	99.80	99.87
Li	8.38	6.49	5.89	17.09	15.10	10.34	7.04	8.92	3.86	19.48	16.84	19.23	17.20	22.83	14.37
Be	0.84	0.72	0.50	1.28	0.93	1.08	1.18	0.75	3.66	19.48	16.84	19.23	1.06	1.07	14.37
V	20.76	21.38	22.70	48.02	33.44	40.58	30.73	19.20	14.24	40.84	25.75	36.85	79.20	147.61	66.26
Cr	10.99	15.67	9.71	25.59	26.64	18.78	11.87	9.86	8.93	34.20	55.55	29.44	111.93	201.04	42.63
Co	3.44	3.81	3.75	6.80	5.59	7.18	4.99	3.68	3.29	10.89	7.79	7.77	14.03	37.06	13.86
Ni	5.23	9.68	8.25	16.56	27.86	17.08	5.13	4.33	9.45	12.14	8.13	5.94	20.84	82.17	12.01
Cu	3.02	5.04	19.99	5.27	7.77	3.55	11.61	3.05	11.95	32.24	3.33	2.06	13.22	101.59	4.38
Zn	36.91	29.61	28.43	51.61	47.10	60.55	51.85	40.81	36.47	68.66	61.95	81.60	71.27	128.54	70.22
Ga	19.03	16.48	13.63	19.91	19.15	18.89	22.54	15.49	13.52	15.19	20.46	15.60	18.19	19.69	17.97
Rb	93.85	111.34	111.73	54.82	115.10	79.24	22.07	110.95	44.49	39.21	70.00	44.53	14.48	14.39	5.93
Sr	278.77	222.19	205.53	330.25	428.20	449.88	869.58	377.05	373.38	456.51	677.51	442.67	474.87	415.79	474.31
Zr	113.94	136.68	56.92	57.47	50.75	40.80	24.83	33.28	70.93	248.84	26.99	253.78	81.80	30.48	21.72
Nb	4.32	2.75	5.05	4.39	5.72	3.51	3.75	5.18	1.30	5.62	1.86	11.25	13.10	9.78	4.27
Sn	0.65	0.82	0.62	0.45	0.53	0.41	0.87	0.46	0.31	0.61	0.46	0.47	0.87	0.77	0.77
Cs	0.62	1.03	0.53	0.63	0.60	0.75	0.18	0.75	0.37	0.62	0.59	0.65	1.30	1.48	1.01
Ba	842.77	988.31	1338.22	856.66	2428.99	1319.21	1248.15	1951.79	320.81	1152.90	1509.41	768.83	772.23	579.27	371.54
La	18.41	14.32	19.41	14.81	34.00	19.66	25.73	11.03	14.10	19.33	26.71	16.84	27.88	18.44	16.61
Ce	27.52	21.03	26.58	21.87	57.76	27.93	45.31	14.38	23.64	28.00	42.47	27.73	47.66	30.38	27.16
Pr	2.61	1.88	2.64	2.21	6.03	2.65	4.90	1.10	2.03	2.64	4.04	2.70	5.19	3.57	3.35
Nd	8.45	5.89	8.95	7.79	21.12	8.71	17.59	3.01	5.50	8.58	13.57	9.39	18.77	13.46	12.59
Sm	1.23	0.71	1.40	1.24	3.19	1.26	2.45	0.31	0.59	1.02	1.75	1.29	2.88	2.00	2.12
Eu	0.75	0.84	0.89	0.92	1.79	1.20	0.98	1.00	0.22	1.15	1.62	1.19	1.18	1.36	1.04
Gd	0.89	0.54	1.19	1.04	2.41	1.02	1.56	0.23	0.41	0.82	1.29	1.04	2.55	1.85	1.90
Tb	0.12	0.07	0.17	0.15	0.33	0.14	0.18	0.04	0.07	0.11	0.17	0.14	0.38	0.27	0.28
Dy	0.48	0.43	0.75	0.76	1.48	0.70	0.60	0.16	0.32	0.49	0.72	0.68	2.03	1.51	1.50
Ho	0.10	0.11	0.14	0.16	0.27	0.14	0.09	0.03	0.06	0.11	0.14	0.15	0.42	0.33	0.31
Er	0.25	0.45	0.36	0.44	0.74	0.35	0.25	0.12	0.20	0.31	0.37	0.45	1.25	1.02	0.87
Tm	0.04	0.09	0.05	0.07	0.09	0.05	0.03	0.02	0.03	0.06	0.05	0.08	0.20	0.17	0.13
Yb	0.27	0.75	0.29	0.44	0.54	0.32	0.16	0.15	0.21	0.42	0.36	0.59	1.31	1.17	0.86
Lu	0.05	0.14	0.04	0.07	0.08	0.05	0.03	0.03	0.04	0.07	0.06	0.11	0.21	0.19	0.13
Y	2.95	3.46	4.35	4.68	7.84	3.84	3.18	1.75	2.09	3.23	3.54	4.05	11.57	8.70	8.33
Sc	2.47	3.73	1.63	6.32	3.36	5.26	2.69	2.68	2.23	4.77	4.41	4.95	11.37	17.85	9.83
Hf	3.99	4.34	1.70	1.67	1.68	1.24	0.74	1.13	1.89	7.30	0.84	6.55	2.34	1.62	0.67
Ta	0.45	0.38	0.44	0.60	0.49	0.29	0.31	0.35	0.04	0.75	0.79	2.94	2.74	0.80	0.68
Tl	0.53	0.58	0.55	0.36	0.55	0.39	0.14	0.51	0.29	0.26	0.34	0.25	0.13	0.11	0.07
Pb	23.65	21.86	20.55	17.63	22.81	18.43	19.37	20.22	15.96	7.48	15.20	5.78	9.76	10.42	7.81
Th	5.43	0.27	2.68	0.42	1.36	0.31	0.14	0.18	4.59	0.40	0.43	5.01	0.51	0.22	0.10

Table 2. Cont.

Sample	D798							1810-1		1814-3			1816-1		
Rock Type	Granitic Gneiss							Tonalitic Gneiss	Trondhjemitic Gneiss			Tonalitic Gneiss			
U	0.53	0.37	0.19	0.17	0.50	0.14	0.07	0.09	0.65	0.31	0.09	0.51	0.26	0.26	0.06
Mg [#]	55.78	48.55	48.45	48.85	51.43	49.73	45.89	50.25	52.04	51.87	52.23	51.39	44.97	45.13	52.05
Eu _N /Eu _{N*}	2.08	3.99	2.05	2.41	1.89	3.13	1.43	10.97	1.29	3.73	3.15	3.03	1.30	2.13	1.55
Sr/Y	94.66	64.29	47.27	70.51	54.65	117.03	273.54	215.45	178.30	141.29	191.28	109.33	41.03	47.80	56.91
La/Yb	68.20	19.02	66.24	33.57	62.62	61.23	158.81	76.08	67.36	46.47	75.03	28.49	21.23	15.70	19.32
Nb/Ta	9.55	7.25	11.56	7.33	11.58	12.05	12.17	14.96	30.37	7.52	2.36	3.83	4.78	12.20	6.25
Zr/Sm	92.33	192.51	40.72	46.46	15.89	32.33	10.13	108.04	119.91	243.96	15.44	196.73	28.40	15.21	10.24
Gd/Yb	3.31	0.71	4.06	2.35	4.44	3.18	9.62	1.61	1.98	1.96	3.62	1.76	1.94	1.58	2.21
Ce/Sr	0.10	0.09	0.13	0.07	0.13	0.06	0.05	0.04	0.06	0.06	0.06	0.06	0.10	0.07	0.06
(La/Yb) _N	45.98	12.82	44.66	22.63	42.22	41.28	107.07	51.29	45.41	31.33	50.58	19.21	14.31	10.59	13.02

$\text{Mg}^{\#} = 100 \times \text{Mg}/(\text{Mg} + \text{Fe}^{2+})$; $\text{TFeO} = \text{TFe}_2\text{O}_3 \times 0.8998$; $\text{Eu}_N/\text{Eu}_N^* = 2 \times \text{Eu}_N/(\text{Sm}_N + \text{Gd}_N)$; N: chondrite normalized; LOI: loss on ignition.

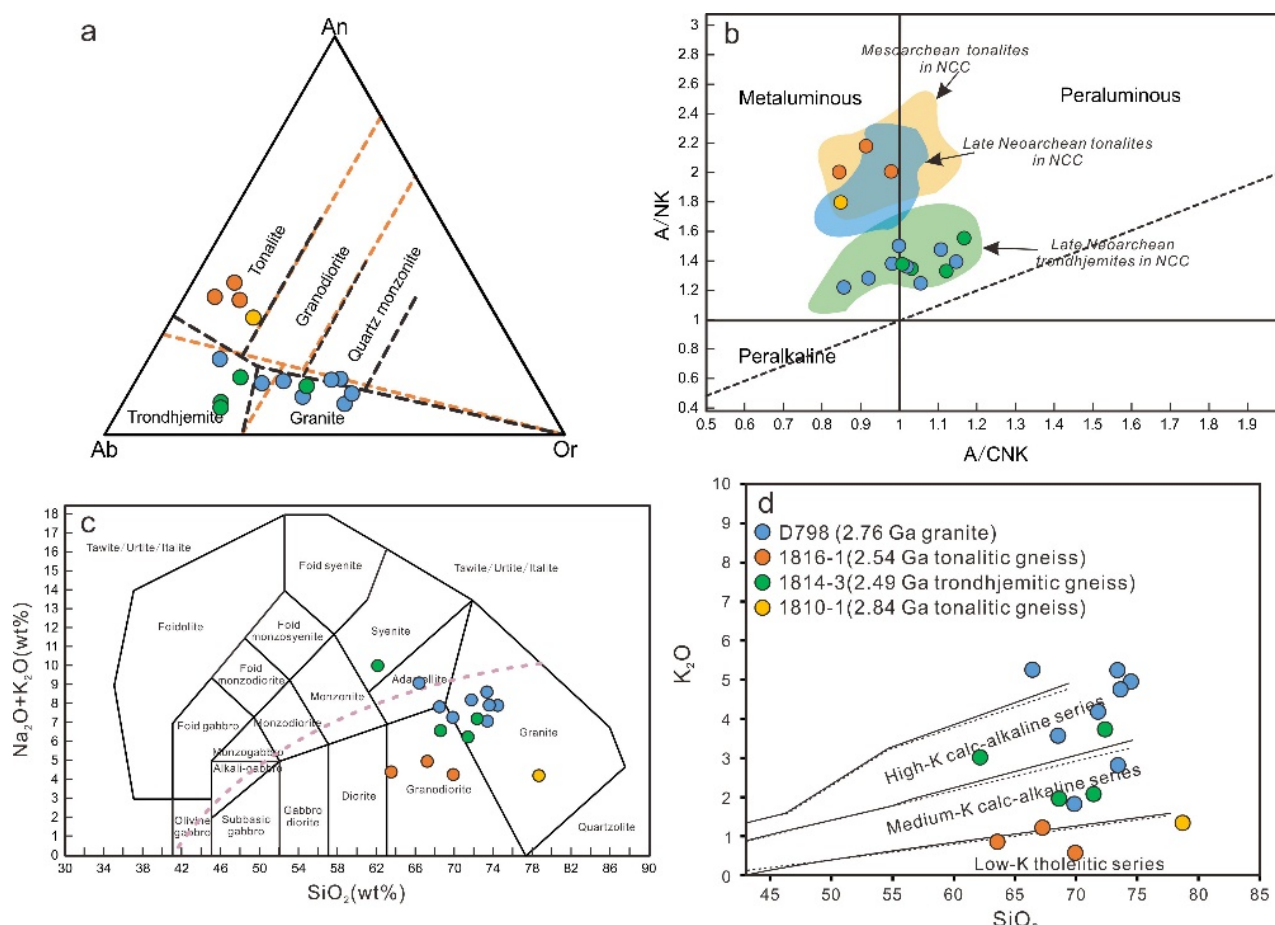


Figure 4. Geochemical discrimination diagrams for the TTG and granitic gneisses from the Diebusige Complex, eastern Alxa Block. (a) An-Ab-Or diagram of the gneiss samples after O’Conner (1965) and Barker (1979); (b) ANK vs. ACNK diagram; (c) SiO₂ vs. total alkali (Na₂O + K₂O) content diagram (Middlemost, 1994); and (d) SiO₂ vs. K₂O diagram.

The 2.76 Ga granitic gneiss (D798) had SiO₂ contents of 64.18–72.30 wt.% (69.63 wt.% on average), Al₂O₃ contents of 12.11–16.18 wt.% (14.37 wt.% on average), and Na₂O/K₂O ratios of 0.59–2.97 (1.15 on average). It displayed high-K calc-alkaline features in the K₂O vs. SiO₂ diagram (Figure 4d) and showed similar characteristics to the 2.5 Ga trondhjemitic gneiss (1814-3) in the TAS diagram and the A/NK vs. A/CNK diagram (Figure 4b,c). This

rock had $Mg^{\#}$ values of 45.89–55.78 (49.87 on average), which are in accordance with the TTG gneisses (Table 2).

4.1.2. Trace Element Geochemistry

In the chondrite-normalized REE diagrams (Figure 5a,c), the TTG gneisses show similar characteristics to the TTG rocks in the NCC. Three TTG gneisses exhibit broadly similar REE distribution patterns and different LREE and HREE fractionation degrees. They all have positive Eu anomalies with $Eu_N/Eu_N^* > 1.29$. The 2.84 Ga tonalitic gneiss ($La_N/Yb_N = 45.41$) and the 2.54 Ga trondhjemite gneiss ($La_N/Yb_N = 19.21$ –50.58, 32.06 on average) show high fractionation between LREEs and HREEs, while the 2.49 Ga tonalitic gneiss shows relatively lower fractionations ($La_N/Yb_N = 10.59$ –14.31, 12.64 on average).

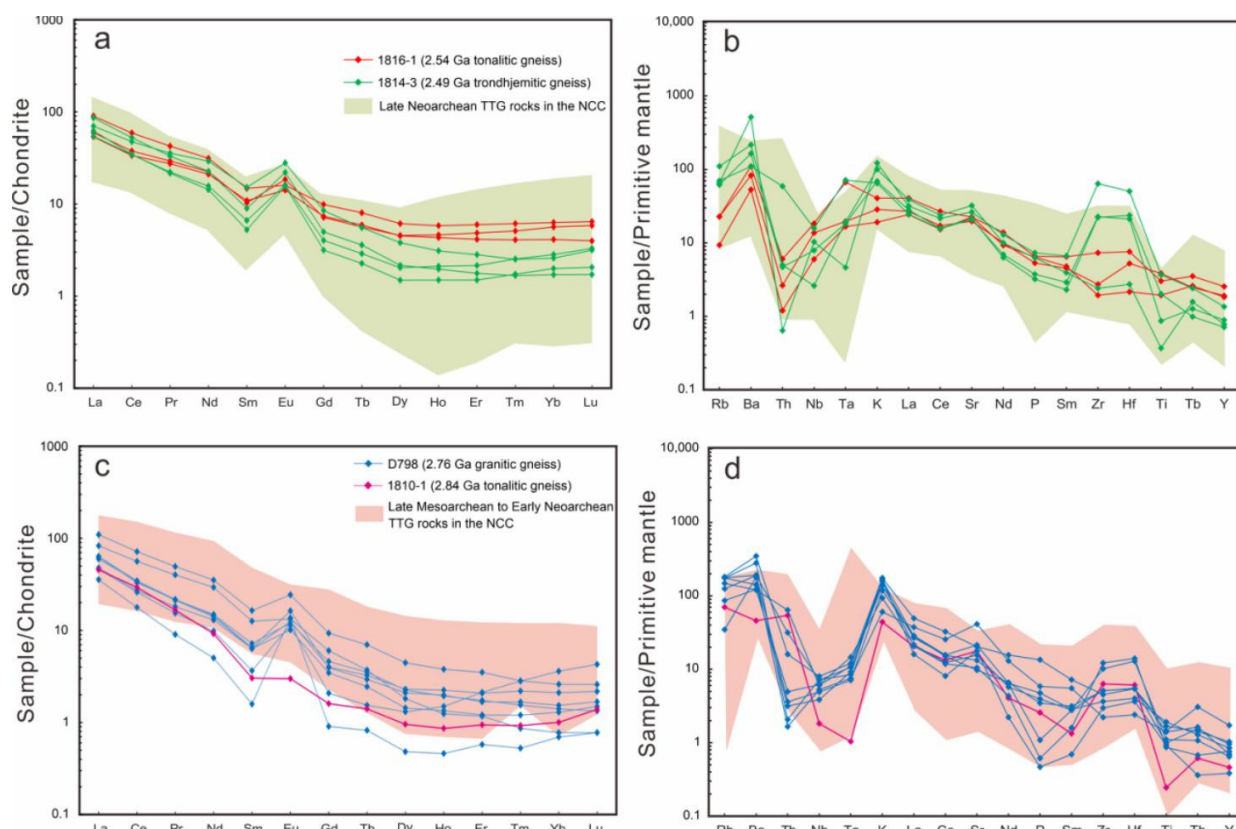


Figure 5. Chondrite-normalized REE patterns (a) and (c) and primitive mantle-normalized spider diagrams (b) and (d) for the TTG and granitic gneisses in the eastern Alxa Block.

In the primitive-normalized trace element diagrams (Figure 5b,d), three TTG gneisses show similar features in enrichment of LILEs (e.g., Rb, Ba, and Sr) and depletion of HFSEs (e.g., Nb, Ta, and Ti). They have variable contents of Cr and Ni. The 2.49 Ga tonalitic gneiss shows much higher Cr (118.5 ppm on average) and Ni (38.3 ppm on average) contents than the 2.54 Ga trondhjemite gneiss (30.2 ppm and 7.8 ppm on average, respectively) and 2.84 Ga tonalitic gneiss (8.9 ppm and 9.4 ppm, respectively). The TTG gneisses and granitic gneisses are characterized by high Sr and low Y contents with high Sr/Y ratios (>41), analogous to average high-SiO₂ adakites and Archean TTG [60].

The 2.76 Ga granitic gneiss exhibits characteristics similar to those of TTG gneisses in REE and trace element patterns (Figure 5c,d) and shows high REE fractionation ($La_N/Yb_N = 12.82$ –107.07, 45.99 on average) and distinctly positive Eu anomalies ($Eu_N/Eu_N^* = 1.43$ –10.97, 3.49 on average). It also shows concentrations of Rb, Ba, and Sr contents and depletions of Nb, Ta, and Ti contents and has low contents of Cr (16.1 ppm on average) and Ni (11.8 ppm on average) that are similar to 2.84 Ga tonalitic gneiss.

4.2. Zircon U-Pb Dating and Hf Isotopic Results

The zircon U-Pb dating results of the TTG and granitic gneiss samples (1810-1, 1814-3, 1816-1, and D798) are presented in Table 3, and representative zircon features are presented in Figure 6. All tested samples contain subhedral–euhedral zircon grains with near oval shapes and arc-shaped terminations. The diameter of zircons from samples 1810-1, 1814-3, 1816-1, and D798 are between 200 μm and 400 μm . Cathodoluminescence (CL) imaging of most zircons reveals core–mantle–rim textures of oscillatory zoned cores overprinted by broad ($<80 \mu\text{m}$) or thin mantle ($<50 \mu\text{m}$) and rim ($<15 \mu\text{m}$) domains (Figure 6). The oscillatory zoned zircon cores are characterized by lower CL brightness values than the rims. Overgrowth mantles and rims are commonly narrow in all samples, with rare grains that are bright gray, homogeneous, and internally structureless. We interpret the zircon cores to have a magmatic origin, with mantles and rims resulting from metamorphic recrystallization [61]. In situ zircon Hf isotope analyses were conducted on the representative zircons of the three TTG gneisses (Figure 6), and the results are listed in Table 3. For the 2.54 Ga tonalitic gneiss (1816-1), the Hf isotopic compositions of the six inherited zircon cores were calculated based on the weighted mean age of $2616 \pm 11 \text{ Ma}$, while the other nineteen magmatic zircon cores were calculated based on the crystallization age of $2540 \pm 38 \text{ Ma}$. Similarly, the Hf isotopic compositions of ten magmatic zircon cores from the 2.49 Ga trondhjemite gneiss (1814-3) were calculated based on the crystallization age of $2491 \pm 18 \text{ Ma}$.

4.2.1. Tonalitic Gneiss Sample 1810-1

Twenty-four analyses were obtained from the tonalitic gneiss sample (1810-1), and three analyses were discordant (spots 1.1, 7.1 and 11.1; Table 3). Two concordant analyses from zircon cores with (spots 6.1 and 15.3) well-preserved oscillatory zoning yield $^{207}\text{Pb}/^{206}\text{Pb}$ ages of $2826 \pm 16 \text{ Ma}$ and $2842 \pm 13 \text{ Ma}$, respectively, with a weighted mean $^{207}\text{Pb}/^{206}\text{Pb}$ age of $2836 \pm 20 \text{ Ma}$ (MSWD = 0.63), which was proposed to be the crystallization age of the protolith (Figure 7a). In addition, there were two $^{207}\text{Pb}/^{206}\text{Pb}$ age groups from the inherited zircon cores that yielded mean $^{207}\text{Pb}/^{206}\text{Pb}$ ages of $2880 \pm 17 \text{ Ma}$ (MSWD = 0.04) and $2918 \pm 8 \text{ Ma}$ (MSWD = 0.80). The weighted mean $^{207}\text{Pb}/^{206}\text{Pb}$ ages of the two Paleoproterozoic age groups obtained from the unzoned rim domains were $1951 \pm 12 \text{ Ma}$ (MSWD = 0.95; 1962–1935 Ma) and $1867 \pm 12 \text{ Ma}$ (MSWD = 1.3; 1915–1843 Ma) (Figure 7a). We considered these two age groups, ca. 1.87 Ga and ca. 1.95 Ga, to represent the ages of metamorphic events [61].

Eight magmatic zircon cores from the 2.84 Ga tonalitic gneiss (1810-1) had $^{176}\text{Hf}/^{177}\text{Hf}$ ratios between 0.280948 and 0.281053 (Table 4), age-corrected $\epsilon_{\text{Hf}}(t)$ values ranging from 1.89 to 1.71, with two-stage Hf model ages (T_{DMC}) of 3111–3242 Ma, respectively. Ten metamorphic zircon mantles or rims had relatively higher $^{176}\text{Hf}/^{177}\text{Hf}$ ratios between 0.281086 and 0.281181 and lower $\epsilon_{\text{Hf}}(t)$ values from -18.90 to -13.49, with two-stage Hf model ages (T_{DMC}) of 3143–3336 Ma.

4.2.2. Trondhjemite Gneiss Sample 1814-3

Of the twenty-seven analyses of zircons from the trondhjemite gneiss sample (1814-3), fourteen from the oscillatory zoned cores yield $^{207}\text{Pb}/^{206}\text{Pb}$ ages ranging between $2191 \pm 24 \text{ Ma}$ and $2577 \pm 21 \text{ Ma}$. Ten analyses (2443–2555 Ma) yield a weighted mean $^{207}\text{Pb}/^{206}\text{Pb}$ age of $2491 \pm 18 \text{ Ma}$ (MSWD = 0.99; Table 3; Figure 7b). Eleven analyses were obtained from the oscillatory unzoned rims and yield $^{207}\text{Pb}/^{206}\text{Pb}$ ages ranging between 1702 Ma and 1943 Ma, with a weighted mean $^{207}\text{Pb}/^{206}\text{Pb}$ age of $1834 \pm 45 \text{ Ma}$ (MSWD = 0.58; Figure 7b). Together with the intercept ages of $1819 \pm 120 \text{ Ma}$ and $2422 \pm 59 \text{ Ma}$ (MSWD = 0.66) (Figure 7b), we consider the mean $^{207}\text{Pb}/^{206}\text{Pb}$ age of $2491 \pm 18 \text{ Ma}$ obtained from the oscillatory zoned cores to represent the crystallization age of the trondhjemite gneiss and the mean $^{207}\text{Pb}/^{206}\text{Pb}$ age of $1834 \pm 45 \text{ Ma}$ obtained from the unzoned rims to represent the age of metamorphism overprinted on the trondhjemite gneiss [61].

Table 3. Zircon U-Pb isotopic data obtained by SHRIMP for TTG and granitic gneisses in the eastern Alxa Block.

Spot No	$^{206}\text{Pb}_\text{c}$ (%)	U ppm	Th ppm	Th/U	$^{206}\text{Pb}^*$ ppm	$^{207}\text{Pb}/^{206}\text{Pb}$	Error in %	$^{207}\text{Pb}/^{235}\text{U}$	Error in %	$^{206}\text{Pb}/^{238}\text{Pb}$	Error in %	Error corr	$^{207}\text{Pb}/^{206}\text{Pb}$	Age (Ma)	$^{206}\text{Pb}/^{238}\text{U}$	Age (Ma)	$^{206}\text{Pb}/^{238}\text{U}$	Discordant (%)
D798: Granitic gneiss																		
1.1	0.94	56	24	0.44	24.1	0.1831	2.7	12.56	3.2	0.4977	1.7	0.533	2681	45	2604	37	3	
2.1	0.37	470	112	0.25	168	0.1600	0.51	9.14	1.2	0.4145	1.1	0.911	2456	8.6	2236	21	9	
2.2	25.34	51	30	0.61	22.9	0.1610	14	7.70	15	0.3520	4.1	0.274	2446	240	1943	67	21	
3.1	0.31	92	77	0.86	35.6	0.1609	1.3	9.98	1.9	0.4499	1.4	0.753	2465	21	2395	29	3	
4.1	0.65	69	77	1.16	29.7	0.1848	1.7	12.69	2.3	0.4983	1.6	0.671	2696	28	2607	33	3	
5.1	2.29	36	24	0.68	9.64	0.1087	6.5	4.52	6.9	0.3018	2.1	0.307	1777	120	1700	31	4	
6.1	1.36	37	19	0.53	12.5	0.1381	5	7.41	6.4	0.3890	3.9	0.616	2202	87	2119	70	4	
7.1	0.52	140	110	0.81	50	0.1599	1.2	9.10	1.8	0.4130	1.4	0.765	2454	20	2229	26	9	
8.1	14.76	52	38	0.74	16.3	0.1010	17	4.19	17	0.3009	2.6	0.149	1643	320	1696	38	-3	
9.1	0.69	74	31	0.43	27.4	0.1567	1.7	9.24	2.3	0.4278	1.6	0.695	2420	29	2296	31	5	
10.1	3.97	31	15	0.51	12	0.1180	7.2	6.94	7.7	0.4270	2.4	0.317	1924	130	2293	46	-19	
11.1	2.33	18	12	0.69	5.71	0.1160	5.9	5.68	6.5	0.3549	2.5	0.389	1895	110	1958	42	-3	
11.2	10.14	53	14	0.27	10.9	0.1350	31	3.90	33	0.2108	4.5	0.139	2159	560	1233	44	43	
12.1	1.16	55	45	0.84	15.3	0.1064	3	4.63	3.4	0.3159	1.7	0.497	1738	54	1769	26	-2	
13.1	1.48	45	29	0.65	13.5	0.1133	3.5	5.34	4	0.3417	1.8	0.464	1852	64	1895	30	-2	
14.1	18.37	31	17	0.56	8.15	0.0810	36	2.80	36	0.2480	3.6	0.098	1211	710	1428	44	-18	
15.1	8.97	165	105	0.66	45.3	0.0990	13	3.91	13	0.2873	1.7	0.133	1597	230	1628	24	-2	
16.1	2.34	46	20	0.45	14.7	0.1090	12	5.45	12	0.3616	2.5	0.201	1788	220	1990	40	-11	
17.1	0.23	210	203	1.00	63.4	0.1234	1.2	5.97	1.9	0.3512	1.4	0.768	2005	21	1940	24	3	
18.1	0.19	121	91	0.78	45.1	0.1730	0.81	10.31	1.6	0.4323	1.4	0.867	2587	14	2316	28	10	
19.1	0.52	147	103	0.72	40.4	0.1073	1.4	4.70	1.9	0.3180	1.3	0.692	1753	25	1780	21	-2	
20.1	0.11	177	146	0.85	81.2	0.1921	0.61	14.11	1.4	0.5326	1.3	0.900	2760	10	2752	28	0	
21.1	0.16	224	222	1.03	90.9	0.1753	0.6	11.39	1.4	0.4712	1.2	0.900	2609	10	2489	25	5	
22.1	0.26	170	1	0.00	81.4	0.1970	0.61	15.09	1.4	0.5557	1.3	0.902	2801	10	2849	29	-2	
23.1	2.51	39	26	0.69	11.6	0.0956	4.7	4.41	5.1	0.3345	1.9	0.372	1539	89	1860	30	-21	
24.1	0.67	140	102	0.75	39.8	0.1054	1.5	4.78	2	0.3286	1.3	0.669	1721	27	1832	21	-6	
25.1	1.23	61	27	0.46	21.3	0.1531	2.8	8.40	3.3	0.3981	1.6	0.499	2380	49	2160	30	9	
26.1	6.87	72	22	0.31	18	0.1220	11	4.47	12	0.2661	2.2	0.192	1985	200	1521	28	23	
1810–1: Tonalitic gneiss																		
1.1	0.07	99	39	0.41	42.4	0.1849	0.78	12.68	1.8	0.4974	1.6	0.902	2697	13	2603	35	4	
2.1	0.01	453	107	0.24	138	0.1186	0.85	5.80	1.4	0.3549	1.2	0.809	1935	15	1958	20	-1	
3.1	0.01	47	102	2.23	13.5	0.1172	1.7	5.35	2.3	0.3310	1.6	0.702	1915	30	1843	26	4	
3.2	0.03	307	176	0.59	88.8	0.1133	0.69	5.26	1.4	0.3368	1.2	0.872	1853	12	1871	20	-1	
3.3	0.12	164	141	0.89	48	0.1158	0.94	5.43	1.6	0.3403	1.3	0.810	1892	17	1888	21	0	
4.1	0.02	184	56	0.31	83.7	0.1935	0.57	14.09	1.4	0.5280	1.3	0.912	2772	9.3	2733	28	1	
4.2	0.01	1102	3	0.00	337	0.1204	0.87	5.90	1.6	0.3557	1.4	0.846	1962	16	1962	23	0	
5.1	0.10	52	49	0.98	14.8	0.1157	2	5.28	2.6	0.3312	1.7	0.640	1890	36	1844	27	2	
6.1	0.01	338	168	0.51	160	0.2000	0.98	15.22	1.5	0.5521	1.2	0.773	2826	16	2834	27	0	
7.1	0.01	771	548	0.74	370	0.2120	0.28	16.32	1.2	0.5584	1.1	0.970	2921	4.5	2860	26	2	
7.2	0.09	76	28	0.38	39.7	0.2073	1.4	17.42	2.4	0.6090	1.9	0.803	2885	23	3068	47	-6	
8.1	0.06	80	56	0.72	21.5	0.1156	1.3	4.95	1.9	0.3104	1.4	0.756	1890	23	1742	22	8	
9.1	0.00	594	127	0.22	165	0.1141	0.56	5.08	1.3	0.3230	1.2	0.900	1866	10	1804	18	3	
10.1	0.00	1373	743	0.56	531	0.1901	0.48	11.80	1.3	0.4503	1.2	0.925	2743	7.8	2397	23	13	
11.1	0.07	91	36	0.41	40.5	0.2098	1.9	14.99	3.7	0.5180	3.2	0.854	2904	31	2691	70	7	
12.1	0.04	123	48	0.40	62.2	0.2185	0.8	17.80	1.7	0.5908	1.5	0.875	2970	13	2993	35	-1	
13.1	0.02	204	77	0.39	97.9	0.2101	0.69	16.17	1.6	0.5581	1.4	0.900	2906	11	2859	33	2	
13.2	0.01	480	205	0.44	238	0.2067	0.56	16.45	1.6	0.5772	1.5	0.938	2880	9.1	2937	36	-2	

Table 3. Cont.

Spot No	$^{206}\text{Pb}_c$ (%)	U ppm	Th ppm	Th/U	$^{206}\text{Pb}^*$ ppm	$^{207}\text{Pb}/^{206}\text{Pb}$	Error in %	$^{207}\text{Pb}/^{235}\text{U}$	Error in %	$^{206}\text{Pb}/^{238}\text{Pb}$	Error in %	Error corr	$^{207}\text{Pb}/^{206}\text{Pb}$	Age (Ma)	$^{206}\text{Pb}/^{238}\text{U}$	Age (Ma)	$^{206}\text{Pb}/^{238}\text{U}$	1 σ	Discordant (%)
14.1	0.03	224	112	0.52	62.8	0.1127	0.95	5.07	1.7	0.3263	1.4	0.818	1843	17	1820	22	1		
14.2	0.09	274	94	0.35	83.1	0.1187	0.86	5.78	1.6	0.3529	1.3	0.835	1937	15	1949	22	-1		
15.1	0.09	94	36	0.40	26.8	0.1130	1.3	5.15	2	0.3304	1.5	0.760	1849	23	1840	24	0		
15.2	0.02	775	11	0.01	239	0.1200	0.46	5.94	1.3	0.3588	1.2	0.931	1957	8.2	1976	20	-1		
15.3	0.02	718	185	0.27	338	0.2020	0.78	15.25	2.5	0.5480	2.4	0.949	2842	13	2816	54	1		
16.1	0.43	26	27	1.07	7.65	0.1148	2.5	5.42	3.2	0.3423	2	0.620	1876	46	1898	33	-1		
1814–3: Trondhjemitic gneiss																			
1.1	0.19	31	31	1.05	12.8	0.1588	1.5	10.68	2.4	0.4879	1.8	0.773	2443	25	2561	38	-5		
2.1	0.12	25	6	0.24	10.6	0.1661	1.7	11.43	2.6	0.4994	2	0.761	2518	28	2611	42	-4		
3.1	0.02	84	86	1.06	34.7	0.1646	0.93	10.87	1.7	0.4788	1.4	0.837	2504	16	2522	30	-1		
3.2	1.15	5	3	0.62	1.56	0.1172	6.3	5.29	7.4	0.3270	4	0.533	1914	110	1825	63	5		
3.3	0.20	20	12	0.62	8.42	0.1698	2.8	11.44	3.6	0.4890	2.3	0.629	2555	47	2564	48	0		
4.1	0.09	26	29	1.13	10.3	0.1557	1.7	9.75	2.6	0.4540	2	0.755	2410	29	2413	39	0		
5.1	0.00	6	2	0.35	1.88	0.1101	4.5	5.39	6	0.3550	4	0.662	1802	82	1959	67	-9		
6.1	0.17	32	18	0.58	13.3	0.1637	1.5	10.97	2.4	0.4861	1.8	0.767	2495	26	2554	39	-2		
6.2	0.28	12	9	0.75	3.44	0.1171	3.5	5.22	4.4	0.3232	2.7	0.611	1913	63	1805	42	6		
7.1	0.36	14	3	0.26	3.91	0.1103	3.3	5.05	4.2	0.3318	2.6	0.611	1805	60	1847	41	-2		
8.1	0.36	10	4	0.49	2.77	0.1081	4.2	5.03	5.1	0.3374	2.9	0.574	1768	76	1874	47	-6		
9.1	0.00	2	1	0.60	0.563	0.1191	7.8	5.93	10	0.3610	6.3	0.631	1943	140	1987	110	-2		
9.2	0.33	15	13	0.89	6.52	0.1645	2.2	11.33	3.5	0.5000	2.7	0.769	2503	37	2612	58	-4		
10.1	0.02	54	41	0.79	18.5	0.1371	1.4	7.52	2.1	0.3981	1.6	0.753	2191	24	2160	29	1		
10.2	-0.23	16	4	0.25	4.66	0.1095	2.8	5.07	3.7	0.3360	2.4	0.657	1791	51	1867	39	-4		
11.1	0.00	33	32	0.98	13.1	0.1593	3.7	10.07	4.2	0.4587	1.9	0.458	2448	63	2434	39	1		
12.1	0.12	40	28	0.73	18.8	0.1811	2.5	13.71	3	0.5493	1.6	0.552	2663	41	2822	37	-6		
13.1	0.09	37	26	0.72	16.1	0.1720	1.3	12.07	2.1	0.5089	1.7	0.803	2577	21	2652	37	-3		
16.1	0.08	103	87	0.87	39	0.1517	0.93	9.2	1.8	0.4397	1.5	0.851	2365	16	2349	30	1		
16.2	0.28	15	10	0.72	4.23	0.1136	3.6	5.22	4.5	0.3332	2.7	0.607	1858	64	1854	44	0		
17.1	1.12	8	3	0.39	2.35	0.1043	7.9	4.8	9.5	0.3340	5.3	0.556	1702	150	1856	85	-9		
18.1	3.93	7	3	0.40	1.85	0.1150	11	4.89	12	0.3070	5.2	0.423	1886	200	1727	79	8		
19.1	0.47	39	20	0.53	15.7	0.1632	2.2	10.57	3.2	0.4700	2.3	0.722	2489	38	2483	48	0		
20.1	0.15	31	22	0.73	14	0.1732	1.5	12.51	2.4	0.5240	1.9	0.795	2588	24	2716	42	-5		
21.1	0.00	22	24	1.15	9.07	0.1601	1.8	10.61	3	0.4800	2.4	0.802	2457	30	2529	50	-3		
22.1	0.00	15	3	0.21	4.15	0.1136	3.2	5.04	4.2	0.3217	2.7	0.646	1857	57	1798	42	3		
23.1	0.27	24	18	0.78	10.2	0.1627	2.8	10.92	3.5	0.4870	2.1	0.613	2484	47	2557	45	-3		
1816–1: Tonalitic gneiss																			
1.1	0.05	80	44	0.56	25.4	0.1365	2	6.96	2.5	0.3699	1.6	0.615	2029	27	2183	35	7		
2.1	0.02	158	131	0.86	47.6	0.1259	1.8	6.11	2.8	0.3516	2.1	0.762	1942	36	2042	32	5		
3.1	0.01	149	116	0.80	52	0.1481	2.2	8.3	2.6	0.4066	1.4	0.523	2200	25	2324	38	5		
4.1	0.03	154	113	0.76	66.8	0.1754	1.1	12.19	1.8	0.5038	1.4	0.776	2630	30	2610	18	-1		
4.2	0.13	140	71	0.53	59.9	0.1740	0.72	11.94	1.5	0.4975	1.3	0.879	2603	29	2597	12	0		
5.1	0.09	85	56	0.69	32.7	0.1593	1	9.86	1.9	0.4488	1.6	0.839	2390	31	2448	17	2		
6.1	0.04	108	54	0.52	44	0.1651	0.87	10.8	2.2	0.4746	2	0.918	2504	42	2508	15	0		
7.1	0.01	355	342	1.00	138	0.1630	0.92	10.17	1.5	0.4523	1.2	0.791	2406	24	2487	16	3		
8.1	0.00	153	88	0.59	67.1	0.1771	0.68	12.47	1.5	0.5105	1.3	0.889	2659	29	2626	11	-1		
9.1	0.02	322	272	0.87	118	0.1524	0.88	8.93	1.8	0.4248	1.6	0.873	2282	30	2373	15	4		

Table 3. Cont.

Spot No	$^{206}\text{Pb}_c$ (%)	U ppm	Th ppm	Th/U	$^{206}\text{Pb}^*$ ppm	$^{207}\text{Pb}/^{206}\text{Pb}$	Error in %	$^{207}\text{Pb}/^{235}\text{U}$	Error in %	$^{206}\text{Pb}/^{238}\text{Pb}$	Error in %	Error corr	$^{207}\text{Pb}/^{206}\text{Pb}$	Age (Ma)	$^{206}\text{Pb}/^{238}\text{U}$	Age (Ma)	Discordant (%)
														1σ	1σ	1σ	
10.1	0.12	110	71	0.67	30.3	0.1080	1.2	4.756	1.9	0.3194	1.4	0.758	1787	22	1766	22	-1
11.1	0.04	88	50	0.58	34	0.1598	1	9.88	1.8	0.4483	1.5	0.824	2388	29	2454	17	3
12.1	0.04	134	107	0.83	55.2	0.1762	0.79	11.67	1.6	0.4804	1.3	0.863	2529	28	2618	13	3
13.1	0.28	82	35	0.44	23.4	0.1141	1.5	5.18	2.1	0.3295	1.5	0.712	1836	24	1866	27	2
14.1	0.04	268	186	0.72	82.6	0.1264	0.88	6.254	1.6	0.3588	1.3	0.826	1977	22	2049	16	4
15.1	0.03	155	123	0.82	63.9	0.1634	1.4	10.8	1.9	0.4794	1.3	0.698	2525	28	2491	23	-1
16.1	0.00	44	27	0.64	12	0.1101	1.9	4.8	2.6	0.3163	1.8	0.691	1772	28	1801	34	2
17.1	0.04	79	50	0.66	35.7	0.1815	0.9	13.2	1.7	0.5275	1.5	0.853	2731	33	2667	15	-2
18.1	0.06	159	120	0.78	49.4	0.1365	1.1	6.8	1.7	0.3615	1.3	0.776	1989	22	2183	19	9
18.2	-0.03	110	61	0.57	46.7	0.1697	1	11.58	1.8	0.4949	1.5	0.822	2592	32	2555	17	-1
19.1	0.00	54	53	1.02	14.8	0.1091	1.7	4.81	2.4	0.3199	1.7	0.700	1789	26	1784	31	0
20.1	0.08	82	42	0.53	34	0.1731	2.2	11.54	2.7	0.4837	1.5	0.552	2543	31	2588	37	2
21.1	0.02	267	208	0.81	92.8	0.1420	2.3	7.92	2.7	0.4047	1.4	0.511	2191	26	2251	40	3
22.1	0.13	65	28	0.44	18	0.1096	1.5	4.85	2.2	0.3210	1.6	0.719	1794	25	1793	28	0
23.1	0.00	159	80	0.52	60.4	0.1578	0.74	9.64	1.6	0.4430	1.4	0.882	2364	27	2432	12	3
24.1	0.11	120	98	0.84	48.5	0.1630	0.85	10.51	1.6	0.4679	1.4	0.851	2474	28	2487	14	0
25.1	0.03	94	67	0.74	34.7	0.1579	1.8	9.33	2.3	0.4286	1.4	0.634	2299	28	2434	30	6
26.1	0.04	199	151	0.78	74.5	0.1590	1.9	9.54	2.5	0.4354	1.7	0.671	2330	33	2445	32	5
27.1	0.39	62	28	0.47	16.9	0.1069	2.1	4.68	2.7	0.3177	1.6	0.613	1778	25	1748	39	-2
28.1	0.04	131	75	0.59	56.5	0.1773	0.75	12.28	1.6	0.5024	1.4	0.888	2624	31	2628	12	0
29.1	0.35	67	33	0.50	18.2	0.1112	1.8	4.8	2.4	0.3132	1.6	0.672	1756	24	1820	32	3
30.1	0.66	265	187	0.73	86	0.1366	1.3	7.08	2.6	0.3757	2.3	0.875	2056	40	2185	22	6

Errors are 1-sigma; Pb_c and Pb^* indicate the common and radiogenic portions, respectively. Error in Standard calibration was 0.22% (not included in above errors but required when comparing data from different mounts). Common Pb corrected using measured ^{204}Pb .



Figure 6. Representative cathodoluminescence images of dated zircons. The white solid-line circle and white number represent the analytical spot of U-Pb dating and dating result, respectively. The yellow dashed-line circle and yellow number represent the analytical spot of Hf isotope and its corrected $^{176}\text{Hf}/^{177}\text{Hf}$ value, respectively.

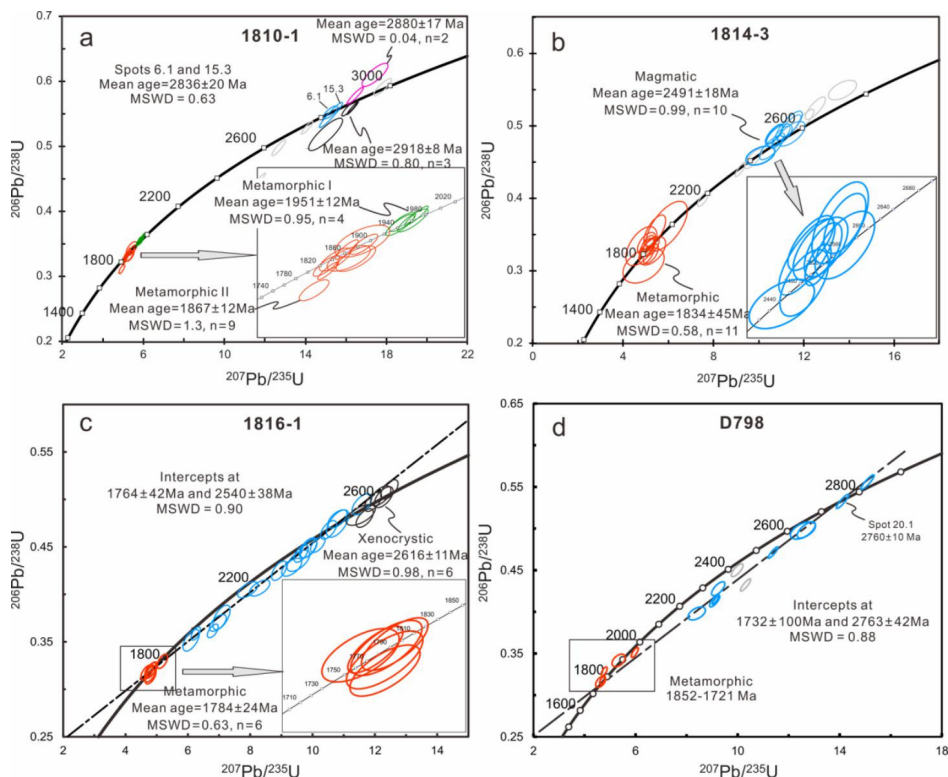


Figure 7. U-Pb concordia diagrams for zircons from the TTG rocks (a–c) and granitic gneiss (d) in the eastern Alxa Block. The purple and black ellipses represent analyses for inherited or xenocrystic zircons; The gray ellipses represent discordant analyses; The blue ellipses represent analyses for magmatic zircons, while the red and green ellipses represent analyses for metamorphic zircons.

Table 4. Lu-Hf isotopic data for zircons from TTG rocks in the eastern Alxa Block.

No.	Measured Age (Ma)	Used Age (Ma)	$^{176}\text{Yb}/^{177}\text{Hf}$	$^{176}\text{Lu}/^{177}\text{Hf}$	$^{176}\text{Hf}/^{177}\text{Hf}$ (corr)	2σ	$\varepsilon_{\text{Hf}}(0)$	$\varepsilon_{\text{Hf}}(t)$	2σ	T_{DM}	T_{DMC}	$f_{\text{Lu/Hf}}$
1810–1: Tonalitic gneiss												
2.1	1935	1935	0.008069	0.000277	0.281181	0.000013	-56.27	-13.49	0.46	2831	3134	-0.99
3.1	1915	1915	0.011251	0.000387	0.281154	0.000014	-57.22	-15.05	0.50	2875	3196	-0.99
3.3	1892	1892	0.009593	0.000331	0.281128	0.000012	-58.13	-16.41	0.44	2905	3246	-0.99
4.1	2772	2772	0.015876	0.000621	0.281053	0.000014	-60.78	0.42	0.48	3027	3111	-0.98
4.2	1962	1962	0.010297	0.000390	0.281165	0.000013	-56.84	-13.62	0.47	2861	3162	-0.99
5.1	1890	1890	0.005287	0.000177	0.281153	0.000013	-57.26	-15.37	0.44	2861	3192	-0.99
6.1	2826	2826	0.029679	0.001094	0.281031	0.000017	-61.55	-0.04	0.61	3094	3178	-0.97
8.1	1890	1890	0.007648	0.000272	0.281133	0.000013	-57.98	-16.23	0.45	2895	3235	-0.99
9.1	1866	1866	0.014119	0.000632	0.281168	0.000014	-56.73	-15.96	0.49	2874	3203	-0.98
10.1	2743	2743	0.032849	0.001155	0.281035	0.000015	-61.42	-1.89	0.54	3094	3203	-0.97
11.1	2904	2904	0.011499	0.000435	0.280979	0.000018	-63.42	1.15	0.64	3112	3182	-0.99
12.1	2970	2970	0.009732	0.000366	0.280948	0.000015	-64.51	1.71	0.53	3148	3208	-0.99
13.1	2906	2906	0.029166	0.001132	0.281010	0.000018	-62.32	0.92	0.63	3127	3195	-0.97
13.2	2880	2880	0.016740	0.000676	0.280963	0.000021	-63.98	-0.45	0.77	3153	3242	-0.98
14.2	1937	1937	0.008957	0.000322	0.281169	0.000014	-56.69	-13.93	0.49	2850	3158	-0.99
15.1	1849	1849	0.008050	0.000352	0.281086	0.000014	-59.61	-18.90	0.50	2962	3336	-0.99
15.3	2842	2842	0.041481	0.001464	0.281023	0.000014	-61.84	-0.68	0.49	3136	3223	-0.96
16.1	1876	1876	0.008185	0.000293	0.281169	0.000015	-56.69	-15.28	0.52	2848	3176	-0.99
1814–3: Trondhjemite gneiss												
1.1	2443	2491	0.023648	0.000801	0.281170	0.000014	-56.65	-2.12	0.49	2884	3011	-0.98
2.1	2518	2491	0.012920	0.000479	0.281123	0.000015	-58.32	-3.25	0.54	2923	3068	-0.99
3.1	2504	2491	0.010837	0.000401	0.281112	0.000016	-58.69	-3.49	0.55	2931	3079	-0.99
3.3	2555	2491	0.023738	0.000807	0.281152	0.000016	-57.29	-2.77	0.55	2909	3043	-0.98
6.1	2495	2491	0.016543	0.000587	0.281137	0.000016	-57.82	-2.93	0.58	2912	3051	-0.98
6.2	1913	1913	0.010601	0.000413	0.281192	0.000018	-55.89	-13.79	0.64	2826	3131	-0.99
8.1	1768	1768	0.008023	0.000293	0.281137	0.000015	-57.81	-18.83	0.54	2890	3269	-0.99
9.2	2503	2491	0.017259	0.000587	0.281112	0.000016	-58.71	-3.83	0.56	2946	3096	-0.98
11.1	2448	2491	0.020314	0.000703	0.281152	0.000015	-57.28	-2.59	0.53	2901	3034	-0.98
19.1	2489	2491	0.011975	0.000419	0.281135	0.000017	-57.90	-2.73	0.61	2903	3041	-0.99
21.1	2457	2491	0.021810	0.000711	0.281134	0.000017	-57.93	-3.26	0.62	2926	3068	-0.98
22.1	1857	1857	0.009303	0.000381	0.281235	0.000019	-54.35	-13.45	0.67	2766	3070	-0.99
23.1	2484	2491	0.017408	0.000619	0.281132	0.000017	-57.99	-3.15	0.62	2921	3062	-0.98
1816–1: Tonalitic gneiss												
1.1	2183	2540	0.008120	0.000341	0.281196	0.000014	-55.73	0.71	0.51	2815	2909	-0.99
2.1	2042	2540	0.018306	0.000719	0.281205	0.000015	-55.40	0.39	0.52	2830	2925	-0.98
3.1	2324	2540	0.019608	0.000785	0.281240	0.000017	-54.16	1.52	0.61	2788	2868	-0.98
4.1	2610	2616	0.019010	0.000764	0.281190	0.000017	-55.94	1.48	0.59	2854	2931	-0.98
4.2	2597	2616	0.007257	0.000312	0.281223	0.000015	-54.77	3.46	0.54	2777	2832	-0.99
5.1	2448	2540	0.008014	0.000324	0.281208	0.000016	-55.30	1.17	0.58	2798	2885	-0.99
6.1	2508	2540	0.007759	0.000320	0.281183	0.000014	-56.18	0.29	0.51	2831	2929	-0.99
7.1	2487	2540	0.037669	0.001519	0.281252	0.000019	-53.76	0.65	0.67	2826	2911	-0.95
8.1	2626	2616	0.008833	0.000360	0.281186	0.000015	-56.09	2.05	0.52	2830	2903	-0.99
9.1	2373	2540	0.025353	0.001020	0.281249	0.000017	-53.86	1.41	0.62	2793	2873	-0.97
10.1	1766	1766	0.008814	0.000354	0.281229	0.000017	-54.58	-15.70	0.59	2773	3110	-0.99
11.1	2454	2540	0.010133	0.000398	0.281209	0.000017	-55.29	1.05	0.61	2803	2891	-0.99
12.1	2618	2616	0.024690	0.000973	0.281204	0.000018	-55.44	1.61	0.63	2851	2925	-0.97
13.1	1866	1866	0.007226	0.000292	0.281215	0.000017	-55.07	-13.87	0.60	2787	3098	-0.99
14.1	2049	2540	0.029831	0.001212	0.281251	0.000017	-53.79	1.15	0.61	2805	2886	-0.96
15.1	2491	2540	0.013793	0.000541	0.281188	0.000017	-56.02	0.07	0.60	2841	2941	-0.98
16.1	1801	1801	0.002951	0.000119	0.281388	0.000015	-48.93	-8.96	0.52	2544	2799	-1.00
17.1	2667	2616	0.010778	0.000429	0.281184	0.000018	-56.16	1.86	0.64	2838	2912	-0.99
18.1	2183	2540	0.017517	0.000689	0.281208	0.000018	-55.30	0.54	0.65	2824	2917	-0.98
18.2	2555	2540	0.011776	0.000483	0.281162	0.000015	-56.95	-0.76	0.55	2872	2982	-0.99
19.1	1784	1784	0.004382	0.000165	0.281405	0.000018	-48.35	-8.82	0.65	2525	2779	-1.00
20.1	2588	2540	0.014708	0.000577	0.281166	0.000015	-56.81	-0.78	0.54	2873	2983	-0.98
21.1	2251	2540	0.023336	0.000939	0.281174	0.000017	-56.49	-1.10	0.62	2888	2999	-0.97
22.1	1793	1793	0.006664	0.000281	0.281417	0.000018	-47.92	-8.32	0.65	2516	2761	-0.99
23.1	2432	2540	0.007641	0.000319	0.281159	0.000016	-57.04	-0.57	0.59	2863	2973	-0.99
24.1	2487	2540	0.017488	0.000671	0.281209	0.000019	-55.26	0.61	0.67	2821	2913	-0.98
25.1	2434	2540	0.011524	0.000450	0.281171	0.000017	-56.63	-0.39	0.60	2857	2964	-0.99
26.1	2445	2540	0.031465	0.001271	0.281214	0.000019	-55.09	-0.26	0.68	2859	2957	-0.96
27.1	1748	1748	0.004465	0.000183	0.281458	0.000022	-46.48	-7.78	0.77	2455	2697	-0.99
28.1	2628	2616	0.014402	0.000576	0.281162	0.000017	-56.95	0.80	0.62	2879	2965	-0.98
29.1	1820	1820	0.007359	0.000304	0.281517	0.000020	-44.39	-4.20	0.71	2383	2574	-0.99
30.1	2185	2540	0.012065	0.000470	0.281174	0.000017	-56.52	-0.31	0.60	2855	2960	-0.99

Note: measured age (Ma) represents the measured age of SHRIMP U-Pb dating for the analyses, and the used age (Ma) represents the ages that are used during the calculation of $\varepsilon_{\text{Hf}}(t)$ and model age. The crustal model ages (T_{DMC}) were calculated by assuming $^{176}\text{Lu}/^{177}\text{Hf}$ ratio of 0.010 for the upper crust.

Ten magmatic zircons from the 2.49 Ga trondhjemite gneiss (1814-3) have $^{176}\text{Hf}/^{177}\text{Hf}$ ratios between 0.281112 and 0.281170 (Table 4), corresponding to age-corrected $\varepsilon_{\text{Hf}}(t)$

values between -3.38 and -2.12 , slightly lower than those of magmatic zircons from sample 1810-1. The two-stage Hf model ages (T_{DMC}) range from 3011 Ma to 3096 Ma. Three analyses from the metamorphic zircon grains or rims present $^{176}\text{Hf}/^{177}\text{Hf}$ ratios varying from 0.281137 to 0.281235, and their age-corrected $\epsilon\text{Hf(t)}$ values are between -18.83 and -13.45 . The corresponding two-stage Hf model ages (T_{DMC}) range from 3070 to 3269 Ma.

4.2.3. Tonalitic Gneiss Sample 1816-1

Thirty-two analyses were obtained from the tonalitic gneiss sample (1816-1) (Table 3; Figure 7c). Six analyses from the inherited cores yield $^{207}\text{Pb}/^{206}\text{Pb}$ ages of 2588–2667 Ma, with a weighted mean age of 2616 ± 11 Ma (MSWD = 0.98; Figure 7c). Eighteen analyses from magmatic zircon cores show variable degrees of Pb loss with $^{207}\text{Pb}/^{206}\text{Pb}$ ages of 2042–2555 Ma, and seven analyses from metamorphic zircons or rims yield $^{207}\text{Pb}/^{206}\text{Pb}$ ages of 1748–1866 Ma. All analyses except for those from inherited zircons define a discordia line with an upper concordia intercept age of 2540 ± 38 Ma and a lower concordia intercept age of 1764 ± 42 Ma (MSWD = 0.90; Figure 7c). Six concordant analyses from unzoned rim domains (spots 10.1, 16.1, 19.1, 22.1, 27.1, and 29.1) that yield $^{207}\text{Pb}/^{206}\text{Pb}$ ages between 1820 ± 32 Ma and 1748 ± 39 Ma have a weighted mean age of 1784 ± 24 Ma (MSWD = 0.63), which is identical to the intercept ages within errors. Therefore, ages of 2540 ± 38 Ma and 1784 ± 24 Ma are proposed to reflect the crystallization and metamorphic ages of the tonalitic gneiss, respectively.

Nineteen magmatic zircon cores from the 2.54 Ga tonalitic gneiss have $^{176}\text{Hf}/^{177}\text{Hf}$ ratios ranging from 0.281159 to 0.281252 (Table 4), age-corrected $\epsilon\text{Hf(t)}$ values from -1.10 to 1.52 , with two-stage Hf model ages (T_{DMC}) ranging from 2868 Ma to 2999 Ma, respectively. Seven metamorphic zircon grains exhibit $^{176}\text{Hf}/^{177}\text{Hf}$ ratios between 0.281215 and 0.281517 and relatively lower $\epsilon\text{Hf(t)}$ values between -15.70 and -4.20 . The corresponding two-stage Hf model ages (T_{DMC}) are 2574–3110 Ma, which are mainly concentrated in the ranges of 2697–2799 Ma, respectively. In addition, six inherited zircon cores show a similar $^{176}\text{Hf}/^{177}\text{Hf}$ ratio range of 0.281162–0.281223, with $\epsilon\text{Hf(t)}$ values of 0.80–3.46 and corresponding two-stage Hf model ages (T_{DMC}) of 2832–2965 Ma.

4.2.4. Granitic Gneiss Sample D798

Twenty-eight analyses were obtained from the granitic gneiss sample (D798) (Table 3; Figure 7d). Twelve analyses show a large error (≥ 87 Ma), which is useless for age determination, and two analyses are discordant (spots 3.1 and 18.1). Nine analyses show variable degrees of Pb loss with $^{207}\text{Pb}/^{206}\text{Pb}$ ages of 2380–2801 Ma and define a discordia line with an upper concordia intercept age of 2763 ± 42 Ma (MSWD = 0.88; Figure 7d). The only analysis (spot 20.1) close to the concordia line that yields a $^{207}\text{Pb}/^{206}\text{Pb}$ age of 2760 ± 10 Ma responds well to the upper intercept age, reflecting the protolith emplacement age of the granitic gneiss. Four analyses from unzoned rims yield $^{207}\text{Pb}/^{206}\text{Pb}$ ages of 1852–1721 Ma and are interpreted as the metamorphic ages of the granitic gneiss [61].

5. Discussion

5.1. Petrogenesis of the TTG Rocks and Granitic Gneiss

The TTG gneisses from the Diebusige Complex are characterized by high SiO_2 contents (>62 wt.%), Sr/Y ratios (41–191) and intermediate $\text{Mg}^{\#}$ values (44.97–52.23) (Table 2), with negative Nb, Ta, and Ti anomalies and enrichment in Sr (Figure 5b,d). These characteristics are similar to those of Archean TTGs and high- SiO_2 adakites, which are consistent with the results in the Sr vs. $(\text{CaO} + \text{Na}_2\text{O})$ diagram (Figure 8a). The low $\epsilon\text{Hf(t)}$ values (-3.83 to 3.46) and the presence of old xenocrystic zircons (2.84 Ga and 2.54 Ga tonalitic gneiss samples) suggest a crustal origin for the protoliths. The moderately to strongly fractionated REE patterns ($(\text{La}/\text{Yb})_N = 10.59$ –50.58), low Sr contents (373.38–677.51 ppm) and positive Eu anomalies ($\text{Eu}_N/\text{Eu}_{N^*} = 1.29$ –3.73)) suggest partial melting in the garnet stability field and the absence of plagioclase in the residue. Generally, rutile has a lower Nb/Ta ratio than chondrite, and its residue in the source or separation and differentiation during magmatic

crystallization led to a higher Nb/Ta ratio of the melts [62]. Element Nb has a higher distribution coefficient than Ta in hornblende [63,64], and the presence of hornblende in the residue led to lower Nb/Ta and Dy/Yb ratios and higher Zr/Sm ratios for the corresponding melts [65]. The 2.49 Ga trondhjemite gneiss and 2.54 Ga tonalitic gneiss in the Langshan area have Nb/Ta ratios lower than those of chondrite (17.6 [66]; 19.9 [67]), indicating that the negative Nb, Ta, and Ti anomalies were not caused by residual rutile in the source but were more likely related to the residues of hornblende in the source. The 2.84 Ga tonalitic gneiss has high Nb/Ta ratios; thus, its negative Nb, Ta, and Ti anomalies may have been controlled by rutile residues in the source. Together with the classification proposed by Moyen (2011) [68], the 2.49 Ga trondhjemite gneiss and 2.54 Ga tonalitic gneiss were derived from partial melting of garnet-bearing amphibolite under high-to-medium pressure conditions, while the 2.84 Ga tonalitic gneiss was derived from partial melting of rutile-bearing eclogite under high-pressure conditions (Figure 8b,c).

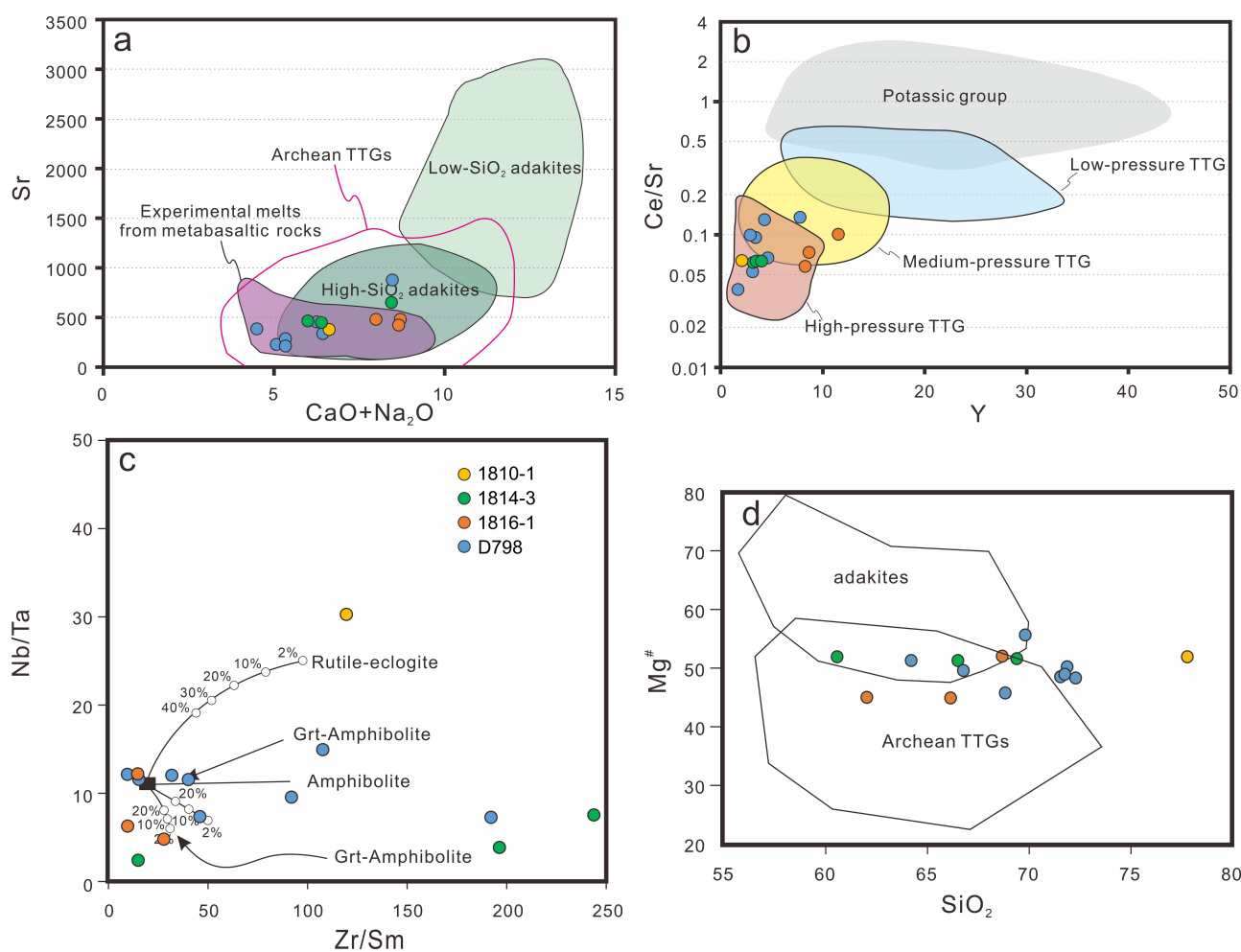


Figure 8. Geochemical modeling results for the TTG and granitic gneisses in the eastern Alxa Block. (a) Sr vs. $(\text{CaO} + \text{Na}_2\text{O})$ diagram after references [60,64,69]; (b) Ce/Sr vs. Y diagram after reference [68]; and (c) Nb/Ta vs. Zr/Sm diagram and melting curves after reference [70]; (d) $\text{Mg}^{\#}$ vs. SiO_2 diagram after reference [71].

The 2.76 Ga granitic gneiss from the Diebusige Complex has SiO_2 contents (66.43–74.49 wt.%), Sr/Y ratios (47–274, 117 on average), and intermediate $\text{Mg}^{\#}$ values (45.89–55.78, 49.87 on average) (Table 2 and Figure 8d), with significantly negative Nb and Ta anomalies and slight Ti anomalies (Figure 5d), which are similar to ca. 2.5 Ga TTG gneisses discussed above and show the features of high- SiO_2 adakites (Figure 8a). High Sr/Y ratios, moderate to strong REE fractionations and positive Eu anomalies ($\text{Eu}_N/\text{Eu}_N^{*}$

= 1.43–10.97) suggest that the granitic gneiss was probably derived from partial melting of a subducted basaltic slab with garnet in the residue. The granitic gneiss shows low Nb/Ta (7.25–14.96, 10.81 on average) and Zr/Sm ratios (10.13–192.51, 67.30 on average), indicating that it was derived from partial melting of garnet-bearing amphibolite (Figure 8c).

Previous studies have suggested that the potential source of Archean TTGs and modern adakites may have been the melting of subducting oceanic crust [2,60,72,73], thickened lower crust [74–76], or delaminated lower crust [74,77]. Generally, TTG or adakitic melts with low Mg[#] values and Cr and Ni concentrations can be generated by the partial melting of mafic rocks underplating the lower crust [69,78], while those generated from the partial melting of a subducting slab and delaminated thickened lower crust would have higher Mg[#] values and MgO, Cr, and Ni contents on account of the interaction with the overlying mantle wedge during ascent [60,74,79,80]. Additionally, TTG melts produced by the partial melting of the delaminated lower crust would have higher contents of MgO (>3 wt.%), TiO₂ (>0.9 wt.%) and compatible elements [81–83]. The low MgO (<3.21 wt.%) and TiO₂ (<0.81 wt.%) contents of TTG gneisses from the Langshan area can rule out the origin of partial melting of the delaminated lower crust. The Mg[#] value can be used as a marker to reflect whether the mafic rock was contaminated by the mantle during the melting process; generally, the Mg[#] value of a typical mid-oceanic ridge basalt is <60 (51 on average), and the Mg[#] value of the melt formed by its partial melting is <45 [69,76]. All TTG gneisses and the granitic gneiss in this study show similar Mg[#] values (approximately 50) (Figure 8d), indicating that a certain degree of mantle contamination may have occurred during the ascent of the TTG melts. However, they have different compatible element compositions: the 2.84 Ga tonalitic gneiss and 2.76 Ga granitic gneiss have low Cr and Ni contents, and the 2.49 Ga trondhjemite and 2.54 Ga tonalitic gneisses have relatively high contents of Cr and Ni. Therefore, the 2.84 Ga tonalitic gneiss and 2.76 Ga granitic gneiss might have formed by the partial melting of the thickened lower crust, whereas the 2.49 Ga trondhjemite and the 2.54 Ga tonalitic gneisses are probably related to the partial melting of the subducted oceanic slab.

5.2. Archean to Late Paleoproterozoic Crustal Evolution in the Alxa Block

The Diebusige Complex is one of the oldest metamorphic series in the eastern Alxa Block. The results show that the 2.84 Ga and 2.54 Ga tonalitic gneisses, the 2.49 Ga trondhjemite, and the 2.76 Ga granitic gneiss are components of the Diebusige Complex. The magmatic zircon age populations at ca. 2.8 Ga and ca. 2.5 Ga indicate that the eastern Alxa Block experienced at least two magmatic events in the late Mesoarchean to late Neoarchean era. Zircon Hf isotope analysis shows that all magmatic zircons from the TTG rocks have $\epsilon_{\text{Hf}}(t)$ values ranging from -3.83 to 3.46, which suggest a crustal origin for the protoliths. Previous studies have suggested that the two-stage zircon Hf model age (T_{DMC}) can accurately reflect the extraction time of source materials from depleted mantle [84]. Magmatic zircons from the 2.84 Ga tonalitic gneiss have T_{DMC} values between 3.24 Ga and 3.11 Ga, while those from the 2.54 Ga tonalitic gneiss and 2.49 Ga trondhjemite gneiss have T_{DMC} values of 3.0–2.83 Ga and 3.10–3.01 Ga, respectively, indicating that the Langshan TTG gneisses were derived from reworking of Paleo-Mesoarchean crust and mixed with mantle materials to different degrees during migration. The 2.84 Ga tonalitic gneiss is the oldest rock currently exposed in the Alxa Block. Recently, Gong et al. (2012) and Zhang et al. (2013b) [51,52] recognized 2.5 Ga TTG rocks from the Beidashan Complex in the western Alxa Block. Zircon Hf isotopic features suggested that the western Alxa Block experienced a mostly 2.8–2.7 Ga crustal growth and a ca. 2.5 Ga magmatic–metamorphic event. The T_{DMC} values of 3.59–3.02 Ga obtained from the ca. 2.8 Ga-inherited zircons also implied the existence of Paleo-Mesoarchean crustal materials in the western Alxa Block [52]. Combined datasets show that the eastern and western Alxa Block probably had the same Paleo-Mesoarchean crust, and the Alxa Block experienced Paleo-Mesoarchean crustal growth, a ca. 2.8 Ga magmatic event, and a ca. 2.5 Ga magmatic–metamorphic event.

The Langshan TTG gneisses and granitic gneiss recorded continuous metamorphic ages of 1962–1721 Ma with peaks at ca. 1.95 Ga and ca. 1.85 Ga. Paleoproterozoic metamorphic events were widely developed in every Precambrian basement in the Alxa Block, such as the Bayanwulashan Complex in the eastern Alxa Block and the Beidashan Complex and Longshoushan Complex in the western Alxa Block [50,52,85,86]. The remaining NCC also recorded these two metamorphic events, and previous studies have suggested that ca. 1.95 Ga and ca. 1.85 Ga corresponded to the formation ages of the Khondalite Belt and the TNCO [27,87–90], respectively. However, whether the formation of the TNCO could have affected the Alxa Block located in the westernmost part of the NCC is still uncertain. A few models suggested the ca. 1.95 Ga and ca. 1.85 Ga events were related to the assembly and breakup of the Paleoproterozoic Columbia supercontinent since they have been identified globally (e.g., Laurentia, Baltica, Amazonia, and India [91–96]).

5.3. Early Geological History of the Alxa Block in Comparison with the YC, TC, and Main NCC

The NCC, YC, and TC are three old cratons in China that constitute the main nucleus of the Chinese continent [5,6,27,97]. Despite considerable progress over recent decades in understanding the Precambrian evolution of these three cratons, limited work has been conducted on comparing their early geological histories [7,8,98–102].

As an important component of the Archean crust, TTG rocks play an important role in the study of Precambrian crustal evolution. In terms of the YC, previous studies show that Paleo-Neoarchean TTG rocks were well developed in the YC [11,13,103–107]. The oldest TTG rocks were formed during 3437–3262 Ma, and zircon Hf isotope studies have suggested that these rocks with $\varepsilon_{\text{Hf}}(t)$ values of −4.7–1.2 were sourced from the Hadean to Eoarchean crust [17–21,103,104] (Figure 9). Additionally, detrital zircons with ages of 3.8–3.2 Ga have been identified in the YC [24,25], indicating that the beginning of crustal evolution of the YC was as early as the Eoarchean to Paleoarchean era (Figures 9 and 10d). Mesoarchean TTG rocks from the YC have $\varepsilon_{\text{Hf}}(t)$ values of −10–3, which yield T_{DMC} values ranging between ca. 3.8 Ga and ca. 3.0 Ga [20,105] (Figure 10f). This suggests that Eoarchean to Paleoarchean crustal materials in the YC were reworked in the Mesoarchean. The Neoarchean rocks were also recognized from the YC [15], and their zircon Hf isotopic features suggest a derivation from Mesoarchean reworked components (Figure 10f).

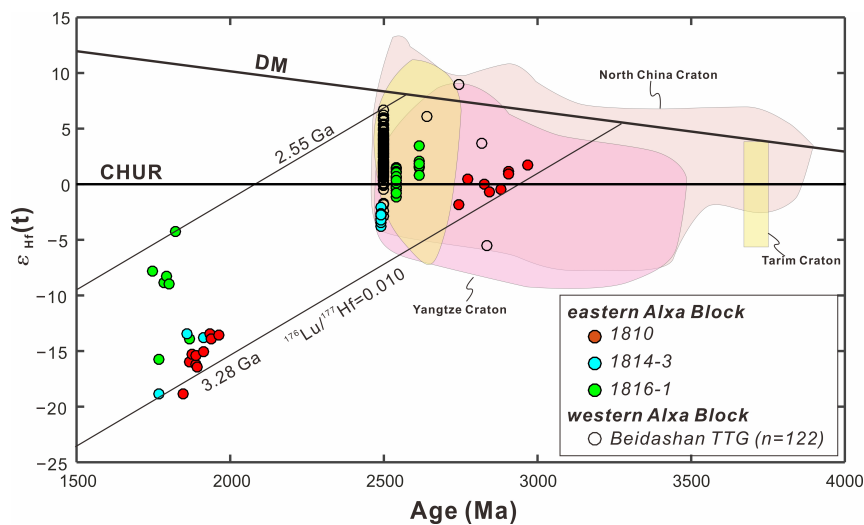


Figure 9. Diagram of $\varepsilon_{\text{Hf}}(t)$ values vs. $^{207}\text{Pb}/^{206}\text{Pb}$ ages for zircons from the basement rocks in the Alxa Block and the main North China, Tarim, and Yangtze cratons. Data for the Alxa Block are from references [51,52] and this study; (2) data for the main North China Craton are from references [30,65,106,108–115]; (3) data for the Tarim Craton are from references [22,23,98,99,116,117]; and (4) data for the Yangtze Craton are from references [11,14,17,19,21,24,102,103,107,118–120].

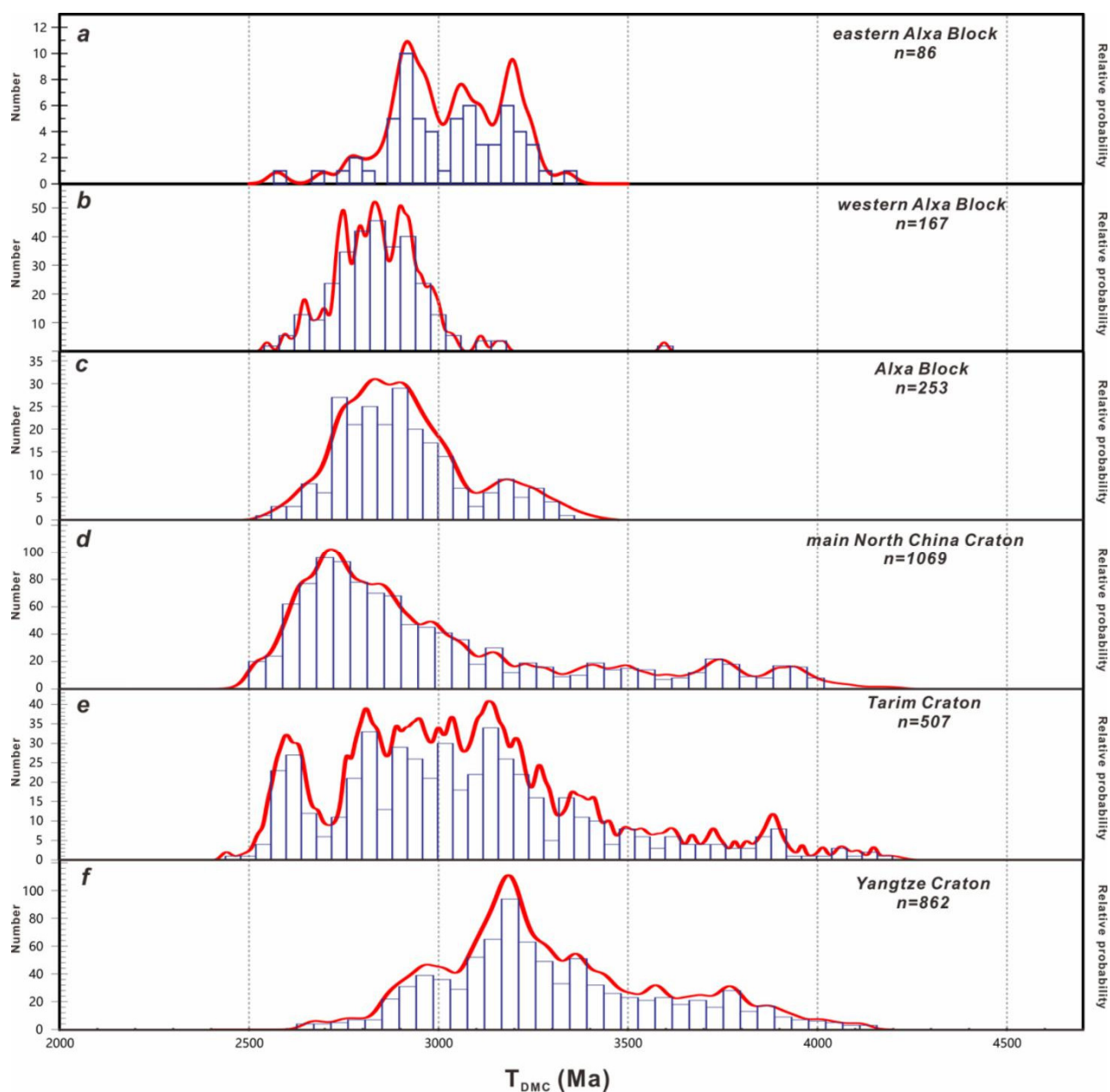


Figure 10. Zircon Hf isotope model age (T_{DMC}) histogram for basement rocks of the eastern Alxa Block (a), western Alxa Block (b), whole Alxa Block (c), and the main North China (d), Tarim (e), and Yangtze (f) cratons. Data sources are the same as those in Figure 9.

The discovery of ca. 3.7 Ga tonalitic gneisses with a mean $\epsilon_{Hf}(t)$ value of -0.7 ± 2.6 suggests that the crustal evolution of the TC began before the Eoarchean era [22] (Figures 9 and 10c). Detrital zircons from metasedimentary rocks in the northern TC were dated ca. 2.5 Ga to ca. 3.5 Ga with T_{DMC} values from ca. 3.9 Ga to ca. 3.7 Ga [23], similarly indicating that the crustal components in the TC may have been generated as early as ca. 3.9 Ga. Neoarchean orthogneisses and mafic–ultramafic rocks are widely exposed in the TC [12,16,95,98,99]. Previous studies have shown that continuous magmatic events occurred in the Neoarchean era, and zircon Hf isotopes yield a large range of $\epsilon_{Hf}(t)$ values (ca. $-8\text{--}10$) with two-stage model ages from the Paleoarchean to Neoarchean era (ca. 3.4–2.8 Ga) [16,23,98,116,117] (Figures 9 and 10c). This suggests that basement rocks in the TC involved synchronous crustal growth and reworking during the Paleo-Neoarchean era.

Numerous detrital and inherited zircons from a variety of metasedimentary rocks in the eastern NCC have been dated 3.88–3.6 Ga, suggesting that the beginning of crustal evolution of the NCC was as early as before the Eoarchean era [30,121–124] (Figure 10d). Recently, ca. 3.8 Ga TTG rocks and granulite enclaves were also identified in the NCC [125,126], further confirming the existence of Eoarchean continental materials and the initial time of crustal evolution of the NCC. Paleoarchean zircons from the eastern NCC have $\epsilon_{\text{Hf}}(t)$ values ranging from −5 to 3 and give Eo-Paleoarchean two-stage model ages varying from 3.9 Ga to 3.4 Ga (Figures 9 and 10b). Zircons from the Mesoarchean and Neoarchean TTG rocks have variable $\epsilon_{\text{Hf}}(t)$ values of −5.5–10.2 (3.6 on average) and −7.8–12.6 (4.1 on average) with two-stage model ages of 4.2–2.8 Ga and 3.9–2.5 Ga, respectively (Figures 9 and 10b). These results indicate that basement rocks in the main NCC involved synchronous crustal growth and reworking, similar to the TC during the Paleo-Neoarchean era.

The Alxa Block is the westernmost component of the NCC. The existence of Archean rocks has long been controversial until ca. 2.5 Ga TTG rocks were identified from the western Alxa Block [51,52]. Mesoarchean to early Paleoproterozoic granitic gneisses (2.76 Ga) and TTG gneisses (2.84 Ga, 2.54 Ga, and 2.49 Ga) from the Langshan area in the eastern Alxa Block are reported in this study. As mentioned above, magmatic zircons from the Langshan TTG gneisses have $\epsilon_{\text{Hf}}(t)$ values ranging from −3.83 to 3.46 and two-stage model ages ranging from 3.3 Ga to 2.9 Ga with peaks at ca. 3.2 Ga and ca. 3.0 Ga. Magmatic zircons from the ca. 2.5 Ga TTG rocks in the western Alxa Block have $\epsilon_{\text{Hf}}(t)$ values varying from −5.54 to 8.98, and two-stage model ages mainly vary from 3.0 Ga to 2.6 Ga, with a peak at ca. 2.8 Ga [51,52]. By contrast (Figures 9 and 10), the eastern Alxa Block recorded a 3.3–2.9 Ga crustal growth and 2.8–2.7 Ga and ca. 2.5 Ga crustal reworking, which have been extensively recorded in most ancient cratons worldwide [31,75,126,127], whereas the western Alxa Block recorded a 2.8–2.7 Ga crustal growth and ca. 2.5 Ga crustal growth and reworking. This indicates that the eastern Alxa Block has older crustal materials than the western Alxa Block, and crustal growth and reworking simultaneously occurred 2.8–2.7 Ga in the Alxa Block (Figure 10a,b). The combination of available datasets suggests that the oldest basement exposed in the Alxa Block formed in the Paleo-Mesoarchean era and that crustal evolution began in the Paleoarchean era, which was younger than those of the main NCC, TC, and YC (Figures 9 and 10). Therefore, we suggest that the Alxa Block probably has its unique crustal evolutionary history before the early Paleoproterozoic.

6. Conclusions

Based on geological, geochronological, geochemical, and zircon Lu-Hf isotope data from the Langshan area in the eastern Alxa Block, we reach the following conclusions:

- (1). The granitic gneiss and three TTG gneisses from the Langshan area were mainly emplaced 2.76 Ga, 2.84 Ga, 2.54 Ga, and 2.49 Ga, respectively, supporting the existence of Archean rocks in the eastern Alxa Block.
- (2). Zircon Lu-Hf isotope data indicated that the Langshan TTG gneisses were derived from partial melting of crustal materials extracted from depleted mantle during the Paleoarchean to Mesoarchean era (3.24–2.83 Ga).
- (3). The eastern Alxa Block experienced an important period of crustal growth during ca. 3.24–2.83 Ga, followed by crustal reworking of ca. 2.8 Ga and ca. 2.5 Ga, and the Alxa Block probably had its unique crustal evolution history from before the early Paleoproterozoic era, which was younger than that of the main NCC, TC, and YC.

Author Contributions: Conceptualization, J.Q. and J.Z.; methodology, B.Z.; software, H.Z.; investigation, P.N., J.Q. and J.Z.; resources, J.Q.; data curation, P.N., B.Z. and H.Z.; writing—original draft preparation, P.N.; writing—review and editing, J.Q. and J.Z.; visualization, P.N., B.Z. and H.Z.; supervision, J.Q.; funding acquisition, J.Q. and J.Z. All authors have read and agreed to the published version of the manuscript.

Funding: This research was funded by: Basic Scientific Research Fund of the Institute of Geology, Chinese Academy of Geological Sciences, grant number J2103; China Geological Survey, grant number DD20230217; National Natural Science Foundation of China, grant number 41972224.

Data Availability Statement: The data presented in this study are available on reasonable request from the corresponding authors.

Acknowledgments: We would like to thank the Key Laboratory of Mineral Resources Evaluation in Northeast Asia, Ministry of Land and Resources of China, the Wuhan Sample Solution Analytical Technology Co., Ltd., and the Beijing SHRIMP Center, Institute of Geology, Chinese Academy of Geological Sciences, Beijing, for their support and assistance on sample processing, zircon U-Pb dating, Hf isotope and major and trace element analyses. The authors are grateful for the critical comments from the anonymous reviewers, which profoundly enhanced the quality of this manuscript.

Conflicts of Interest: The authors declare no conflict of interest.

References

1. Jahn, B.; Glikson, A.Y.; Peucat, J.J.; Hickman, A.H. REE geochemistry and isotopic data of Archean silicic volcanics and granitoids from the Pilbara block, western Australia: Implications for early crustal evolution. *Geochim. Cosmochim. Acta* **1981**, *45*, 1633–1652. [[CrossRef](#)]
2. Moyen, J.-F.; Martin, H. Forty years of TTG research. *Lithos* **2012**, *148*, 312–336. [[CrossRef](#)]
3. Condie, K.C. Episodic growth and supercontinents: A mantle avalanche connection? *Earth Planet. Sci. Lett.* **1998**, *163*, 91–108. [[CrossRef](#)]
4. Condie, K.C. Episodic continental growth models: After thoughts and extensions. *Tectonophysics* **2000**, *322*, 153–162. [[CrossRef](#)]
5. Lu, S.; Zhao, G.; Wang, H.; Hao, G. Precambrian metamorphic basement and sedimentary cover of the North China Craton: A review. *Precambrian Res.* **2008**, *160*, 77–93. [[CrossRef](#)]
6. Zhao, G.; Wilde, S.A.; Cawood, P.A.; Lu, L. Thermal Evolution of Archean Basement Rocks from the Eastern Part of the North China Craton and Its Bearing on Tectonic Setting. *Int. Geol. Rev.* **1998**, *40*, 706–721. [[CrossRef](#)]
7. Zhao, G.C. Paleoproterozoic assembly of the North China Craton. *Geol. Mag.* **2001**, *138*, 89–91. [[CrossRef](#)]
8. Zhao, G.; Wilde, S.A.; Cawood, P.A.; Sun, M. Archean blocks and their boundaries in the North China Craton: Lithological, geochemical, structural and P-T path constraints and tectonic evolution. *Precambrian Res.* **2001**, *107*, 45–73. [[CrossRef](#)]
9. Zhao, G.; Sun, M.; Wilde, S.A.; Li, S. Late Archean to Paleoproterozoic evolution of the North China Craton: Key issues revisited. *Precambrian Res.* **2005**, *136*, 177–202. [[CrossRef](#)]
10. Zhai, M.G.; Guo, J.H.; Liu, W.J. Neoarchean to Paleoproterozoic continental evolution and tectonic history of the North China Craton: A review. *J. Asian Earth Sci.* **2005**, *24*, 547–561. [[CrossRef](#)]
11. Chen, Q.; Sun, M.; Zhao, G.; Zhao, J.; Zhu, W.; Long, X.; Wang, J. Episodic crustal growth and reworking of the Yudongzi terrane, South China: Constraints from the Archean TTGs and potassic granites and Paleoproterozoic amphibolites. *Lithos* **2019**, *326–327*, 1–18. [[CrossRef](#)]
12. Chen, S.; Guo, Z.; Huang, W. Traces of Archean Subduction in the Tarim Craton, Northwest China: Evidence from the Tuoge Complex and Implications for Basement Formation. *J. Geol.* **2019**, *127*, 323–341. [[CrossRef](#)]
13. Huang, M.; Cui, X.; Ren, G.; Guo, J.; Ren, F.; Pang, W.; Chen, F. The 2.73 Ga I-type granites in the Lengshui Complex and implications for the Neoarchean tectonic evolution of the Yangtze Craton. *Int. Geol. Rev.* **2019**, *62*, 649–664. [[CrossRef](#)]
14. Wu, Y.B.; Zhou, G.Y.; Gao, S.; Liu, X.C.; Zheng, Q.; Wang, H.; Yang, J.Z.; Yang, S.H. Petrogenesis of Neoarchean TTG rocks in the Yangtze Craton and its implication for the formation of Archean TTGs. *Precambrian Res.* **2014**, *254*, 73–86. [[CrossRef](#)]
15. Wang, K.; Li, Z.X.; Dong, S.W.; Cui, J.J.; Han, B.F.; Zheng, T.; Xu, Y.L. Early crustal evolution of the Yangtze Craton, South China: New constraints from zircon U-Pb-Hf isotopes and geochemistry of ca. 2.9–2.6 Ga granitic rocks in the Zhongxiang Complex. *Precambrian Res.* **2018**, *314*, 325–352. [[CrossRef](#)]
16. Cai, Z.; Jiao, C.; He, B.; Qi, L.; Ma, X.; Cao, Z.; Xu, Z.; Chen, X.; Liu, R. Archean–Paleoproterozoic tectonothermal events in the central Tarim Block: Constraints from granitic gneisses revealed by deep drilling wells. *Precambrian Res.* **2020**, *347*, 105776. [[CrossRef](#)]
17. Chen, K.; Gao, S.; Wu, Y.; Guo, J.; Hu, Z.; Liu, Y.; Zong, K.; Liang, Z.; Geng, X. 2.6–2.7 Ga crustal growth in Yangtze craton, South China. *Precambr. Res.* **2013**, *224*, 472–490. [[CrossRef](#)]
18. Chen, W.T.; Zhou, M.-F.; Zhao, X.-F. Late Paleoproterozoic sedimentary and mafic rocks in the Hekou area, SW China: Implication for the reconstruction of the Yangtze Block in Columbia. *Precambrian Res.* **2013**, *231*, 61–77. [[CrossRef](#)]
19. Jiao, W.; Wu, Y.; Yang, S.; Peng, M.; Wang, J. The oldest basement rock in the Yangtze Craton revealed by zircon U-Pb age and Hf isotope composition. *Sci. China Ser. D Earth Sci.* **2009**, *52*, 1393–1399. [[CrossRef](#)]
20. Li, Y.H.; Zheng, J.P.; Ping, X.Q.; Xiong, Q.; Xiang, L.; Zhang, H. Complex growth and reworking processes in the Yangtze cratonic nucleus. *Precambrian Res.* **2018**, *311*, 262–277. [[CrossRef](#)]
21. Zhang, S.B.; Zheng, Y.F.; Wu, Y.B.; Zhao, Z.F.; Gao, S.; Wu, F.Y. Zircon U-Pb age and Hf isotope evidence for 3.8 Ga crustal remnant and episodic reworking of Archean crust in South China. *Earth Planet. Sci. Lett.* **2006**, *252*, 56–71. [[CrossRef](#)]

22. Ge, R.; Zhu, W.; Wilde, S.A.; Wu, H. Remnants of Eoarchean continental crust derived from a subducted proto-arc. *Sci. Adv.* **2018**, *4*, eaao3159. [[CrossRef](#)] [[PubMed](#)]
23. Ge, R.; Zhu, W.; Wilde, S.A.; He, J. Zircon U–Pb–Lu–Hf–O isotopic evidence for ≥ 3.5 Ga crustal growth, reworking and differentiation in the northern Tarim Craton. *Precambrian Res.* **2014**, *249*, 115–128. [[CrossRef](#)]
24. Zhang, S.B.; Zheng, Y.F.; Wu, Y.B.; Zhao, Z.F.; Gao, S.; Wu, F.Y. Zircon isotope evidence for ≥ 3.5 Ga continental crust in the Yangtze craton of China. *Precambrian Res.* **2006**, *146*, 16–34. [[CrossRef](#)]
25. Zheng, J.; Griffin, W.; O'Reilly, S.Y.; Zhang, M.; Pearson, N.; Pan, Y. Widespread Archean basement beneath the Yangtze craton. *Geology* **2006**, *34*, 417–420. [[CrossRef](#)]
26. Wan, Y.S.; Liu, D.Y.; Dong, C.Y.; Xie, H.Q.; Kröner, A.; Ma, M.Z.; Liu, S.J.; Xie, S.W.; Ren, P. Formation and Evolution of Archean Continental Crust of the North China Craton. In *Precambrian Geology of China*; Zhai, M., Ed.; Springer: Berlin/Heidelberg, Germany, 2015; pp. 59–136. [[CrossRef](#)]
27. Shen, Q.; Geng, Y.; Song, B.; Wan, Y. New information from the surface outcrops and deep crust of Archean rocks of the North China and Yangtze blocks, and Qinling-Dabie orogenic belt. *Acta Geol. Sin.* **2005**, *79*, 616–627.
28. Niu, P.F.; Qu, J.F.; Zhang, J. Precambrian tectonic affinity of the southern Langshan area, northeastern margin of the Alxa Block: Evidence from zircon U–Pb dating and Lu–Hf Isotopes. *Acta Geol. Sin.* **2022**, *96*, 1516–1533. [[CrossRef](#)]
29. Jahn, B.; Auvray, B.; Shen, Q.; Liu, D.; Zhang, Z.; Dong, Y.; Ye, X.; Zhang, Q.; Cornichet, J.; Mace, J. Archean crustal evolution in China: The Taishan complex, and evidence for juvenile crustal addition from long-term depleted mantle. *Precambrian Res.* **1988**, *38*, 381–403. [[CrossRef](#)]
30. Wu, F.Y.; Zhang, Y.B.; Yang, J.H.; Xie, L.W.; Yang, Y.H. Zircon U–Pb and Hf isotopic constraints on the Early Archean crustal evolution in Anshan of the North China Craton. *Precambrian Res.* **2008**, *167*, 339–362. [[CrossRef](#)]
31. Zhai, M.G.; Santosh, M. The early Precambrian odyssey of the North China Craton: A synoptic overview. *Gondwana Res.* **2011**, *20*, 6–25. [[CrossRef](#)]
32. Zhao, G.; Sun, M.; Wilde, S.A.; Li, S. A Paleo-Mesoproterozoic supercontinent: Assembly, growth and breakup. *Earth-Sci. Rev.* **2004**, *67*, 91–123. [[CrossRef](#)]
33. Zhao, G.; Cawood, P.A.; Li, S.; Wilde, S.A.; Sun, M.; Zhang, J.; He, Y.; Yin, C. Amalgamation of the North China Craton: Key issues and discussion. *Precambrian Res.* **2012**, *222–223*, 55–76. [[CrossRef](#)]
34. Li, J.H.; Qian, X.L.; Huang, C.N.; Liu, S.W. Tectonic framework of North China Block and its cratonization in the Early Precambrian. *Acta Petrol. Sin.* **2000**, *16*, 1–10. (In Chinese)
35. Lu, L.Z.; Xu, X.C.; Liu, F.L. *Early Precambrian Khondalite Series in North China*; Changchun Publishing House: Changchun, China, 1996. (In Chinese)
36. Zhai, M.G. Precambrian tectonic evolution of the North China Craton. *Geol. Soc. Lond. Spec. Publ.* **2004**, *226*, 57–72. [[CrossRef](#)]
37. Bai, J.; Huang, X.G.; Dai, F.Y.; Wu, C.H. *The Precambrian Evolution of China*, 2nd ed.; Geological Publishing House: Beijing, China, 1996; pp. 36–38. (In Chinese)
38. Ma, X.H. *Precambrian Tectonic Framework and Research Methods in China*; Geological Publishing House: Beijing, China, 1987. (In Chinese)
39. Sun, D.Z.; Li, H.M.; Lin, Y.X.; Zhou, H.F.; Zhao, F.Q.; Tang, M. Precambrian geochronology, chronological framework and model of chronocrustal structures of Zhongtiao Mountains. *Acta Geol. Sin.* **1991**, *3*, 20–35. (In Chinese)
40. Wu, C.H. Metasedimentary rocks and tectonic division of North China Craton. *Geol. J. China Univ.* **2007**, *13*, 442–457. (In Chinese)
41. Zhao, G.; Wilde, S.; Cawood, P.A.; Sun, M. SHRIMP U–Pb zircon ages of the Fuping Complex: Implications for Late Archean to Paleoproterozoic accretion and assembly of the North China Craton. *Am. J. Sci.* **2002**, *302*, 191–226. [[CrossRef](#)]
42. Wang, Z.-Z.; Han, B.-F.; Feng, L.-X.; Liu, B.; Zheng, B.; Kong, L.-J. Tectonic attribution of the Langshan area in western Inner Mongolia and implications for the Neoarchean–Paleoproterozoic evolution of the Western North China Craton: Evidence from LA-ICP-MS zircon U–Pb dating of the Langshan basement. *Lithos* **2016**, *261*, 278–295. [[CrossRef](#)]
43. Zhang, J.; Li, J.; Xiao, W.; Wang, Y.; Qi, W. Kinematics and geochronology of multistage ductile deformation along the eastern Alxa block, NW China: New constraints on the relationship between the North China Plate and the Alxa block. *J. Struct. Geol.* **2013**, *57*, 38–57. [[CrossRef](#)]
44. Yang, Z.D.; Pan, X.S.; Yang, Y.F. *Geological Structure Characteristics and Deposites of Alxa Blocks and Adjacent Region*; Science Press: Beijing, China, 1988; pp. 1–254. (In Chinese)
45. Li, J.J. Regional Metallogenic System of Alashan Block in Inner Mongolia Autonomous Region. Ph.D. Thesis, China University of Geoscience, Beijing, China, 2006. (In Chinese).
46. Geng, Y.S.; Wang, X.S.; Shen, Q.H.; Wu, C.M. Redefinition of the Alxa Group complex (Precambrian metamorphic basement) in the Alxa area, Inner Mongolia. *Geol. China* **2006**, *33*, 138–145. (In Chinese)
47. Geng, Y.S.; Wang, X.S.; Shen, Q.H.; Wu, C.M. Chronology of the Precambrian metamorphic series in the Alxa area, Inner Mongolia. *Geol. China* **2007**, *34*, 251–261. (In Chinese)
48. Geng, Y.S.; Zhou, X.W. Early Neoproterozoic granite events in Alxa area of Inner Mongolia and their geological significance: Evidence from geochronology. *Acta Petrol. Mineral.* **2010**, *29*, 779–795. (In Chinese)
49. Geng, Y.S.; Shen, Q.H.; Ren, L.D. Late Neoarchean to Early Paleoproterozoic magmatic events and tectonothermal systems in the North China Craton. *Acta Petrol. Sin.* **2010**, *26*, 1945–1966. (In Chinese)

50. Dan, W.; Li, X.H.; Guo, J.H.; Liu, Y.; Wang, X.C. Paleoproterozoic evolution of the eastern Alxa Block, westernmost North China: Evidence from in situ zircon U-Pb dating and Hf-O isotopes. *Gondwana Res.* **2012**, *21*, 838–864. [[CrossRef](#)]
51. Gong, J.; Zhang, J.; Yu, S.; Li, H.; Hou, K. Ca. 2.5 Ga TTG rocks in the western Alxa Block and their implications. *Chin. Sci. Bull.* **2012**, *57*, 4064–4076. [[CrossRef](#)]
52. Zhang, J.X.; Gong, J.H.; Yu, S.Y.; Li, H.K.; Hou, K.J. Neoarchean-Paleoproterozoic multiple tectonothermal events in the western Alxa block, North China Craton and their geological implication: Evidence from zircon U-Pb ages and Hf isotopic composition. *Precambrian Res.* **2013**, *235*, 36–57. [[CrossRef](#)]
53. Williams, I.S. U-Th-Pb geochronology by ion microprobe. In *Applications of Microanalytical Techniques to Understanding Mineralizing Processes*; McKibben, M.A., Shanks, W.C., Ridley, W.I., Eds.; Economic Geology Publishing Co.: Littleton, CO, USA, 1998; Volume 7, pp. 1–35.
54. Black, L.P.; Kamo, S.L.; Allen, C.M.; Aleinikoff, J.N.; Davis, D.W.; Korsch, R.J.; Foudoulis, C. TEMORA 1: A new zircon standard for Phanerozoic U–Pb geochronology. *Chem. Geol.* **2003**, *200*, 155–170. [[CrossRef](#)]
55. Ludwig, K.R. Manual for Isoplot 3.0: A Geochronological Toolkit for Microsoft Excel. *Berkeley Geochronol. Cent. Spec. Publ.* **2003**, *4*, 1–71.
56. Zhang, S.-H.; Zhao, Y.; Ye, H.; Hu, G.-H. Early Neoproterozoic emplacement of the diabase sill swarms in the Liaodong Peninsula and pre-magmatic uplift of the southeastern North China Craton. *Precambrian Res.* **2016**, *272*, 203–225. [[CrossRef](#)]
57. Paton, C.; Hellstrom, J.; Paul, B.; Woodhead, J.; Herget, J. Iolite: Freeware for the visualisation and processing of mass spectrometric data. *J. Anal. At. Spectrom.* **2011**, *26*, 2508–2518. [[CrossRef](#)]
58. Wu, F.-Y.; Yang, Y.-H.; Xie, L.-W.; Yang, J.-H.; Xu, P. Hf isotopic compositions of the standard zircons and baddeleyites used in U–Pb geochronology. *Chem. Geol.* **2006**, *234*, 105–126. [[CrossRef](#)]
59. Sláma, J.; Košler, J.; Condon, D.J.; Crowley, J.L.; Gerdes, A.; Hanchar, J.M.; Horstwood, M.S.A.; Morris, G.A.; Nasdala, L.; Norberg, N.; et al. Plešovice zircon—A new natural reference material for U–Pb and Hf isotopic microanalyses. *Chem. Geol.* **2008**, *249*, 1–35. [[CrossRef](#)]
60. Martin, H.; Smithies, R.; Rapp, R.; Moyen, J.-F.; Champion, D. An overview of adakite, tonalite–trondhjemite–granodiorite (TTG), and sanukitoid: Relationships and some implications for crustal evolution. *Lithos* **2005**, *79*, 1–24. [[CrossRef](#)]
61. Grant, M.L.; Wilde, S.A.; Wu, F.Y.; Yang, J.H. The application of zircon cathodoluminescence imaging, Th-U–Pb chemistry and U–Pb ages in interpreting discrete magmatic and high-grade metamorphic events in the North China Craton at the Archean/Proterozoic boundary. *Chem. Geol.* **2009**, *261*, 155–171. [[CrossRef](#)]
62. Xiong, X.; Adam, J.; Green, T. Rutile stability and rutile/melt HFSE partitioning during partial melting of hydrous basalt: Implications for TTG genesis. *Chem. Geol.* **2005**, *218*, 339–359. [[CrossRef](#)]
63. Green, T.H. Significance of Nb/Ta as an indicator of geochemical processes in the crust–mantle system. *Chem. Geol.* **1995**, *120*, 347–359. [[CrossRef](#)]
64. Rapp, R.P.; Shimizu, N.; Norman, M.D. Growth of early continental crust by partial melting of eclogite. *Nature* **2003**, *425*, 605–609. [[CrossRef](#)]
65. Huang, X.L.; Niu, Y.; Xu, Y.G.; Yang, Q.J.; Zhong, J.W. Geochemistry of TTG and TTG-like gneisses from Lushan-Taihua complex in the southern North China Craton: Implications for late Archean crustal accretion. *Precambrian Res.* **2010**, *182*, 43–56. [[CrossRef](#)]
66. Jochum, K.P.; Stolz, A.J.; McOrist, G. Niobium and tantalum in carbonaceous chondrites: Constraints on the solar system and primitive mantle niobium/tantalum, zirconium/nobium, and niobium/uranium ratio. *Meteorit. Planet. Sci.* **2000**, *35*, 229–235. [[CrossRef](#)]
67. Münker, C.; Pfänder, J.A.; Weyer, S.; Büchl, A.; Kleine, T.; Mezger, K. Evolution of Planetary Cores and the Earth-Moon System from Nb/Ta Systematics. *Science* **2003**, *301*, 84–87. [[CrossRef](#)]
68. Moyen, J.F. The composite Archean grey gneisses: Petrological significance, and evidence for a non-unique tectonic setting for Archean crustal growth. *Lithos* **2011**, *123*, 21–36. [[CrossRef](#)]
69. Rapp, R.; Shimizu, N.; Norman, M.; Applegate, G. Reaction between slab-derived melts and peridotite in the mantle wedge: Experimental constraints at 3.8 GPa. *Chem. Geol.* **1999**, *160*, 335–356. [[CrossRef](#)]
70. Shan, H.; Zhai, M.; Dey, S. Petrogenesis of Two Types of Archean TTGs in the North China Craton: A Case Study of Intercalated TTGs in Lushan and Non-intercalated TTGs in Hengshan. *Acta Geol. Sin.—Engl. Ed.* **2016**, *90*, 2049–2065. [[CrossRef](#)]
71. Condie, K.C. TTGs and adakites: Are they both slab melts? *Lithos* **2005**, *80*, 33–44. [[CrossRef](#)]
72. Drummond, M.S.; Defant, M.J.; Kepezhinskas, P.K.; Brown, M.; Candela, P.; Peck, D.; Stephens, W.; Walker, R.; Zen, E.-A. Petrogenesis of Slab-Derived Trondhjemite–Tonalite–Dacite/Adakite Magmas. *Trans. R. Soc. Edinb.—Earth Sci.* **1996**, *87*, 205–215. [[CrossRef](#)]
73. Martin, H. Adakitic magmas: Modern analogues of Archaean granitoids. *Lithos* **1999**, *46*, 411–429. [[CrossRef](#)]
74. Bédard, J.H. A catalytic delamination-driven model for coupled genesis of Archaean crust and sub-continental lithospheric mantle. *Geochim. Cosmochim. Acta* **2006**, *70*, 1188–1214. [[CrossRef](#)]
75. Condie, K.C.; Beyer, E.; Belousova, E.; Griffin, W.; O’reilly, S.Y. U–Pb isotopic ages and Hf isotopic composition of single zircons: The search for juvenile Precambrian continental crust. *Precambrian Res.* **2005**, *139*, 42–100. [[CrossRef](#)]
76. Smithies, R. The Archaean tonalite–trondhjemite–granodiorite (TTG) series is not an analogue of Cenozoic adakite. *Earth Planet. Sci. Lett.* **2000**, *182*, 115–125. [[CrossRef](#)]

77. Zegers, T.E.; van Keken, P.E. Middle Archean continent formation by crustal de-lamination. *Geology* **2001**, *29*, 1083–1086. [[CrossRef](#)]
78. Rapp, R.P.; Watson, E.B. Dehydratation melting of metabasalt at 8–32 kbar: Implications for continental growth and crust-mantle recycling. *J. Petrol.* **1995**, *36*, 891–931. [[CrossRef](#)]
79. Smithies, R.H.; Champion, D.C. The Archaean high-Mg diorite suite: Links to tonalite–trondhjemite–granodiorite magmatism and implications for early Archaean crustal growth. *J. Petrol.* **2000**, *41*, 1653–1671. [[CrossRef](#)]
80. Moyen, J.F. High Sr/Y and La/Yb ratios: The meaning of the “adakitic signature”. *Lithos* **2009**, *112*, 556–574. [[CrossRef](#)]
81. Castillo, P.R. An overview of adakite petrogenesis. *Chin. Sci. Bull.* **2006**, *51*, 257–268. [[CrossRef](#)]
82. Wang, Q.; Wyman, D.A.; Xu, J.; Zhao, Z.; Jian, P.; Zi, F. Partial Melting of Thickened or Delaminated Lower Crust in the Middle of Eastern China: Implications for Cu-Au Mineralization. *J. Geol.* **2007**, *115*, 149–161. [[CrossRef](#)]
83. Xu, J.F.; Shinjo, R.; Defant, M.J.; Wang, Q.; Rapp, R.P. Origin of Mesozoic adakitic intrusive rocks in the Ningzhen area of east China: Partial melting of delaminated lower continental crust? *Geology* **2002**, *30*, 1111–1114. [[CrossRef](#)]
84. Wu, F.Y.; Li, X.H.; Zheng, Y.F.; Gao, S. Lu-Hf isotopic systematics and their applications in petrology. *Acta Petrol. Sin.* **2007**, *23*, 185–220. (In Chinese)
85. Dong, C.Y.; Liu, D.Y.; Li, J.J.; Wan, Y.S.; Zhou, H.Y.; Li, C.D.; Yang, Y.H.; Xie, L.W. New evidences from the Bayanwulashan-Helanshan region for the formation age of Khondalite Belt: SHRIMP zircon dating and Hf isotopic composition. *Chin. Sci. Bull.* **2007**, *52*, 1913–1922. (In Chinese) [[CrossRef](#)]
86. Dong, C.; Wan, Y.; Wilde, S.A.; Xu, Z.; Ma, M.; Xie, H.; Liu, D. Earliest Paleoproterozoic supracrustal rocks in the North China Craton recognized from the Daqingshan area of the Khondalite Belt: Constraints on craton evolution. *Gondwana Res.* **2014**, *25*, 1535–1553. [[CrossRef](#)]
87. Kröner, A.; Wilde, S.A.; Li, J.H.; Wang, K.Y. Age and evolution of a late Archean to early Palaeozoic upper to lower crustal section in the Wutaishan/Hengshan/Fuping terrain of northern China. *J. Asian Earth Sci.* **2005**, *24*, 577–595. [[CrossRef](#)]
88. Santosh, M.; Tsunogae, T.; Ohyama, H.; Sato, K.; Li, J.; Liu, S. Carbonic metamorphism at ultrahigh-temperatures: Evidence from North China Craton. *Earth Planet. Sci. Lett.* **2008**, *266*, 149–165. [[CrossRef](#)]
89. Wilde, S.A.; Zhao, G.C.; Sun, M. Development of the North China Craton during late Archean and its final amalgamation at 1.8 Ga: Some speculations on its position within a global palaeoproterozoic supercontinent. *Gondwana Res.* **2002**, *5*, 85–94. [[CrossRef](#)]
90. Zhao, G.C.; Wilde, S.A.; Sun, M.; Li, S.Z.; Li, X.P.; Zhang, J. SHRIMP U-Pb zircon ages of granitoid rocks in the Lvliang Complex: Implications for the accretion and evolution of the Trans-North China Orogen. *Precambrian Res.* **2008**, *160*, 213–226. [[CrossRef](#)]
91. Condie, K.C.; Aster, R.C. Episodic zircon age spectra of orogenic granitoids: The supercontinent connection and continental growth. *Precambrian Res.* **2010**, *180*, 227–236. [[CrossRef](#)]
92. Rogers, J.J.; Santosh, M. Configuration of Columbia, a Mesoproterozoic Supercontinent. *Gondwana Res.* **2002**, *5*, 5–22. [[CrossRef](#)]
93. Rogers, J.J.; Santosh, M. Tectonics and surface effects of the supercontinent Columbia. *Gondwana Res.* **2009**, *15*, 373–380. [[CrossRef](#)]
94. Santosh, M. Assembling North China Craton within the Columbia supercontinent: The role of double-sided subduction. *Precambrian Res.* **2010**, *178*, 149–167. [[CrossRef](#)]
95. Zhang, C.L.; Li, H.K.; Santosh, M.; Li, Z.X.; Zou, H.B.; Wang, H.; Ye, H. Precambrian evolution and cratonization of the Tarim Block, NW China: Petrology, geochemistry, Nd isotopes and U-Pb zircon geochronology from Archean gabbro-TTG-potassic granite suite and Paleoproterozoic metamorphic belt. *J. Asian Earth Sci.* **2012**, *47*, 5–20. [[CrossRef](#)]
96. Zhao, G.C.; Cawood, P.A. Precambrian geology of China. *Precambrian Res.* **2012**, *222*, 13–54. [[CrossRef](#)]
97. Qiu, Y.M.; Gao, S.; McNaughton, N.J.; Groves, D.I.; Ling, W.L. First evidence of >3.2 Ga continental crust in the Yangtze craton of south China and its implications for Archean crustal evolution and Phanerozoic tectonics. *Geology* **2000**, *28*, 11–14. [[CrossRef](#)]
98. Ge, R.F.; Zhu, W.B.; Wilde, S.A.; Wu, H.L.; He, J.W.; Zheng, B.H. Archean magmatism and crustal evolution in the northern Tarim Craton: Insights from zircon U-Pb-Hf-O isotopes and geochemistry of ~2.7 Ga orthogneiss and amphibolite in the Korla Complex. *Precambrian Res.* **2014**, *252*, 145–165. [[CrossRef](#)]
99. Long, X.P.; Chao, Y.; Sun, M.; Zhao, G.C.; Xiao, W.J.; Wan Yu, J.; Yang, Y.H.; Hu, A.Q. Archean crustal evolution of the northern Tarim craton, NW China: Zircon U-Pb and Hf isotopic constraints. *Precambrian Res.* **2010**, *180*, 272–284. [[CrossRef](#)]
100. Wan, Y.S.; Zhang, Z.Q.; Wu, J.S.; Song, B.; Liu, D.Y. Geochemical and Nd isotopic characteristic of some rocks from the Paleoarchean Chentaigou supracrustal, Anshan area, NE China. *Cont. Dyn.* **1997**, *2*, 39–46.
101. Wan, Y.S.; Dong, C.Y.; Ren, P.; Bai, W.Q.; Xie, H.Q.; Liu, S.J.; Xie, S.W.; Liu, D.Y. Spatial and temporal distribution, compositional characteristics and formation and evolution of Archean TTG rocks in the North China Craton: A synthesis. *Acta Petrol. Sin.* **2017**, *33*, 1405–1419. (In Chinese)
102. Zhang, S.-B.; Zheng, Y.-F.; Wu, Y.-B.; Zhao, Z.-F.; Gao, S.; Wu, F.-Y. Zircon U-Pb age and Hf-O isotope evidence for Paleoproterozoic metamorphic event in South China. *Precambrian Res.* **2006**, *151*, 265–288. [[CrossRef](#)]
103. Guo, J.-L.; Gao, S.; Wu, Y.-B.; Li, M.; Chen, K.; Hu, Z.-C.; Liang, Z.-W.; Liu, Y.-S.; Zhou, L.; Zong, K.-Q.; et al. 3.45 Ga granitic gneisses from the Yangtze Craton, South China: Implications for Early Archean crustal growth. *Precambrian Res.* **2014**, *242*, 82–95. [[CrossRef](#)]
104. Guo, J.-L.; Wu, Y.-B.; Gao, S.; Jin, Z.-M.; Zong, K.-Q.; Hu, Z.-C.; Chen, K.; Chen, H.-H.; Liu, Y.-S. Episodic Paleoproterozoic (3.3–2.0 Ga) granitoid magmatism in Yangtze Craton, South China: Implications for late Archean tectonics. *Precambrian Res.* **2015**, *270*, 246–266. [[CrossRef](#)]

105. Qiu, X.-F.; Ling, W.-L.; Liu, X.-M.; Lu, S.-S.; Jiang, T.; Wei, Y.-X.; Peng, L.-H.; Tan, J.-J. Evolution of the Archean continental crust in the nucleus of the Yangtze block: Evidence from geochemistry of 3.0 Ga TTG gneisses in the Kongling high-grade metamorphic terrane, South China. *J. Asian Earth Sci.* **2018**, *154*, 149–161. [[CrossRef](#)]
106. Wu, M.; Zhao, G.; Sun, M.; Li, S.; Bao, Z.; Tam, P.Y.; Eizenhöfer, P.R.; He, Y. Zircon U–Pb geochronology and Hf isotopes of major lithologies from the Jiaodong Terrane: Implications for the crustal evolution of the Eastern Block of the North China Craton. *Lithos* **2014**, *190–191*, 71–84. [[CrossRef](#)]
107. Zhou, G.; Wu, Y.; Li, L.; Zhang, W.; Zheng, J.; Wang, H.; Yang, S. Identification of ca. 2.65 Ga TTGs in the Yudongzi complex and its implications for the early evolution of the Yangtze Block. *Precambrian Res.* **2018**, *314*, 240–263. [[CrossRef](#)]
108. Diwu, C.; Sun, Y.; Guo, A.; Wang, H.; Liu, X. Crustal growth in the North China Craton at ~2.5Ga: Evidence from in situ zircon U–Pb ages, Hf isotopes and whole-rock geochemistry of the Dengfeng complex. *Gondwana Res.* **2011**, *20*, 149–170. [[CrossRef](#)]
109. Geng, Y.S.; Yang, C.H.; Du, L.L.; Ren, L.D.; Song, H.X. Late Neoarchean magmatism and crustal growth in eastern Hebei: Constraint from geochemistry, zircon U–Pb ages and Hf isotope. *Acta Petrol. Sin.* **2018**, *34*, 1058–1082. (In Chinese)
110. Kang, J.L.; Wang, H.C.; Xiao, Z.B.; Sun, Y.W.; Zeng, L.; Pang, Z.B.; Li, J.R. Neoarchean crustal accretion of the North China Craton: Evidence from the TTG gneisses and monzogranitic gneisses in Yunzhong Mountain area, Shanxi. *Acta Petrol. Sin.* **2017**, *33*, 2881–2898.
111. Liu, J.H.; Liu, F.L.; Ding, Z.J.; Liu, C.H.; Yang, H.; Liu, P.H.; Wang, F.; Meng, N. The growth, reworking and metamorphism of early Precambrian crust in the Jiaobei terrane, the North China Craton: Constraints from U–Th–Pb and Lu–Hf isotopic systematics, and REE concentrations of zircon from Archean granitoid gneisses. *Precambrian Res.* **2013**, *224*, 287–303. [[CrossRef](#)]
112. Luo, Z.X.; Huang, X.L.; Wang, Y.; Yang, F.; Han, L. Geochronology and Geochemistry of the TTG Gneisses from the Taihua Group in the Xiaoshan Area, North China Craton: Constraints on Petrogenesis. *Geotecton. Metallog.* **2018**, *42*, 332–347. (In Chinese)
113. Song, H.X.; Yang, C.H.; Du, L.L.; Ren, L.D.; Geng, Y.S. Delineation of the ~2.7 Ga TTG gneisses in Zanhuan Complex, Hebei Province, and its geological significance. *Acta Petrol. Sin.* **2018**, *34*, 1599–1611. (In Chinese)
114. Wang, W.; Zhai, M.G.; Li, T.S.; Santosh, M.; Zhao, L.; Wang, H.Z. Archean-Paleoproterozoic crustal evolution in the eastern North China Craton: Zircon U–Th–Pb and Lu–Hf evidence from the Jiaobei terrane. *Precambrian Res.* **2014**, *241*, 146–160. [[CrossRef](#)]
115. Zhang, S.-B.; Tang, J.; Zheng, Y.-F. Contrasting Lu–Hf isotopes in zircon from Precambrian metamorphic rocks in the Jiaodong Peninsula: Constraints on the tectonic suture between North China and South China. *Precambrian Res.* **2014**, *245*, 29–50. [[CrossRef](#)]
116. Zhang, J.X.; Yu, S.Y.; Gong, J.H.; Li, H.K.; Hou, K.J. The latest Neoarchean-Paleoproterozoic evolution of the Dunhuang block, eastern Tarim craton, northwestern China: Evidence from zircon U–Pb dating and Hf isotopic analyses. *Precambrian Res.* **2013**, *226*, 21–42. [[CrossRef](#)]
117. Zong, K.; Liu, Y.; Zhang, Z.; He, Z.; Hu, Z.; Guo, J.; Chen, K. The generation and evolution of Archean continental crust in the Dunhuang block, northeastern Tarim craton, northwestern China. *Precambrian Res.* **2013**, *235*, 251–263. [[CrossRef](#)]
118. Zhou, G.; Wu, Y.; Gao, S.; Yang, J.; Zheng, J.; Qin, Z.; Wang, H.; Yang, S. The 2.65 Ga A-type granite in the northeastern Yangtze craton: Petrogenesis and geological implications. *Precambrian Res.* **2015**, *258*, 247–259. [[CrossRef](#)]
119. Hui, B.; Dong, Y.; Cheng, C.; Long, X.; Liu, X.; Yang, Z.; Sun, S.; Zhang, F.; Varga, J. Zircon U–Pb chronology, Hf isotope analysis and whole-rock geochemistry for the Neoarchean-Paleoproterozoic Yudongzi complex, northwestern margin of the Yangtze craton, China. *Precambrian Res.* **2017**, *301*, 65–85. [[CrossRef](#)]
120. Wang, Z.; Deng, Q.; Duan, T.; Yang, F.; Du, Q.; Xiong, X.; Liu, H.; Cao, B. 2.85 Ga and 2.73 Ga A-type granites and 2.75 Ga trondhjemite from the Zhongxiang Terrain: Implications for early crustal evolution of the Yangtze Craton, South China. *Gondwana Res.* **2018**, *61*, 1–19. [[CrossRef](#)]
121. Liu, D.Y.; Nutman, A.P.; Compston, W.; Wu, J.S.; Shen, Q.H. Remnants of ≥3800 Ma crust in the Chinese part of the Sino-Korean craton. *Geology* **1992**, *20*, 339–342. [[CrossRef](#)]
122. Liu, D.Y.; Wan, Y.S.; Wu, J.S.; Wilde, S.A.; Dong, C.Y.; Zhou, H.Y.; Yin, X.Y. Archean Crustal evolution and the oldest rocks in the North China Craton. *Geol. Bull. China* **2007**, *26*, 1131–1138. (In Chinese)
123. Liu, D.; Wilde, S.; Wan, Y.; Wu, J.; Zhou, H.; Dong, C.; Yin, X. New U–Pb and Hf isotopic data confirm Anshan as the oldest preserved segment of the North China Craton. *Am. J. Sci.* **2008**, *308*, 200–231. [[CrossRef](#)]
124. Song, B.; Nutman, A.P.; Liu, D.Y.; Wu, J.S. 3800 to 2500 Ma crustal evolution in the Anshan area of Liaoning Province, northern China. *Precambrian Res.* **1996**, *78*, 79–94. [[CrossRef](#)]
125. Wan, Y.S.; Xie, H.Q.; Wang, H.C.; Li, P.C.; Chu, H.; Xiao, Z.B.; Dong, C.Y.; Liu, S.J.; Li, Y.; Hao, G.M.; et al. Discovery of ~3.8 Ga TTG rocks in eastern Hebei, North China Craton. *Acta Geol. Sin.* **2021**, *95*, 1321–1333. (In Chinese)
126. Condie, K.C.; Belousova, E.; Griffin, W.; Sircombe, K.N. Granitoid events in space and time: Constraints from igneous and detrital zircon age spectra. *Gondwana Res.* **2009**, *15*, 228–242. [[CrossRef](#)]
127. Jiang, N.; Guo, J.H.; Zhai, M.G.; Zhang, S.Q. 2.7 Ga crust growth in the North China craton. *Precambrian Res.* **2010**, *179*, 37–49. [[CrossRef](#)]

Disclaimer/Publisher’s Note: The statements, opinions and data contained in all publications are solely those of the individual author(s) and contributor(s) and not of MDPI and/or the editor(s). MDPI and/or the editor(s) disclaim responsibility for any injury to people or property resulting from any ideas, methods, instructions or products referred to in the content.